NASA Technical Paper 1739

Evaluation of a Bulk Calorimeter and Heat Balance for Determination of Supersonic Combustor Efficiency

C. R. McClinton and G. Y. Anderson

DECEMBER 1980

NASA

NASA Technical Paper 1739

Evaluation of a Bulk Calorimeter and Heat Balance for Determination of Supersonic Combustor Efficiency

C. R. McClinton and G. Y. Anderson
Langley Research Center
Hampton, Virginia

National Aeronautics
and Space Administration

**Scientific and Technical
Information Branch**

1980

SUMMARY

Results are presented from the checkout runs of a bulk calorimeter. The calorimeter is designed to quench the combustion at the exit of a direct-connect, hydrogen-fueled, scramjet combustor model, and to provide measurements necessary to perform an analysis of combustion efficiency. Details of the hardware, instrumentation, and calorimetric analysis are presented. The analysis method accounts for the transient nature of the various heat fluxes involved in the calorimetric balance. In the present tests the heat balance is shown to be accurate within ±2 percent, the calculated combustion efficiency varies in a regular way from 0.45 to 0.95 with combustor model parameters (such as injected fuel-equivalence ratio), and the calorimeter appears to quench combustion. The calculated combustion efficiency is repeatable within ±3 percent, and the calorimeter response is rapid enough to allow two fuel settings in a 15-second run. Thus, the bulk calorimeter can be applied as a useful tool in scramjet combustor research.

INTRODUCTION

Efficient hypersonic flight will require a new propulsive device. The leading candidate is the supersonic combustion ramjet, or scramjet engine discussed in reference 1. Several research-size scramjet engines have been successfully ground tested (ref. 2) and have proven the engine cycle potential. Results of these engine studies were incorporated in the NASA Langley Research Center modular engine concept discussed in reference 3. The original combustor concept for the modular engine, discussed in reference 4, is based on previous scramjet engine experience and experimental studies performed in a combustion-heated, oxygen-replenished, direct-connect combustor test stand at Langley Research Center. This test stand is discussed in reference 5. These direct-connect tests are continuing, and they play an important role in the ongoing engine development effort (ref. 6) and basic combustion research. Basic combustion investigations have been performed with a wide range of combustor models, including models with fuel injected from walls (refs. 7 to 10) and struts (refs. 11 and 12). Some of these investigations were conducted to study the effects on combustion of fuel temperature (ref. 13), sweep (refs. 14 and 15), and jet interaction (refs. 9, 10, and 12). Other investigations were conducted to study ignition (ref. 16) and flameholding.

Analysis of combustor performance in the referenced tests has generally relied on two diagnostic techniques: (1) Wall pressure measurements to deduce combustion efficiency using a one-dimensional analysis (ref. 11), and (2) gas-sample and pitot-pressure measurements at the combustor exit to provide fuel distribution, and mixing and combustion efficiency. (See ref. 17 for general procedure and ref. 12 for minor modifications to analysis.) Both of these diagnostic techniques have limited applicability to the high-temperature-reacting two- or three-dimensional flows being analyzed. Several alternative diagnostic techniques have been studied, including nonintrusive measurements such as

infrared emission (ref. 18) and sodium line reversal, and a bulk heat measuring device such as the calorimeter discussed in reference 19.

This report includes a description and evaluation of a bulk calorimeter illustrated in figure 1. The calorimeter design, instrumentation, and analysis technique closely follows that described in reference 19.[1] Conceptually, the calorimeter quenches the reaction with a combination of metered water spray and rapid expansion, converts all the water to gas, and thoroughly mixes all the flow constituents to a uniform mixture. Then the total temperature of the mixture is measured by thermocouple probes. Combustion efficiency of the injected fuel is determined by a calorimetric balance of the entire facility-combustor-calorimeter apparatus, and is available immediately following each test run.

SYMBOLS

A	wall area, m^2
c	specific heat, J/kg-K
d	jet diameter, m
E_F	energy available in fuel, J
E_p	energy released from fuel, J
E'_p	indicated energy released from fuel, J
E_{TG}	energy of test gas, J
H	enthalpy, J/kg
ΔH_R	heat of reaction, J/kg
ΔH_v	heat of vaporization, J/kg
h	total flow height ahead of step, 0.0329 m
h_s	inlet isolation step height 0.00483 m
M	Mach number
m	mass, kg
N	calculated combustion efficiency (see eq. 19)

[1]The authors gratefully acknowledge the assistance of Paul Waltrup and Dick Orth of the Johns Hopkins Applied Physics Laboratory in designing the calorimeter used in this study.

n	number of fuel jets
p	pressure, MPa
Q	heat, J
R	correlation coefficient
r	calorimeter radial location, m
S	jet lateral spacing, m
S_F	fraction of total fuel ($\phi_1 + \phi_2$) injected from downstream injector (ϕ_2)
T	temperature, K
t	tare, fractional error in calorimeter analysis of test-gas energy
x	longitudinal location, m
x_s	distance from step to upstream injector, m
η_c	combustion efficiency, fraction of fuel which has reacted
η_c'	tare-corrected combustion efficiency (see eq. (15))
η_m	mixing efficiency, fraction of fuel which would react if complete chemical reaction occurred without additional mixing
θ	calorimeter circumferential location, rad
μ	molecular weight
τ	time, sec
ϕ	fuel equivalence ratio, ratio of fuel mass fraction to that required for stoichiometric mixture

Subscripts:

b	burner
c	calorimeter
f	total fuel condition (1 + 2)
m	model
n	nozzle

p	calorimeter exit probe
q	quench water
t	stagnation property
w	wall
1	upstream fuel
2	downstream fuel

A bar over a symbol refers to mass-averaged values. A dot over a symbol refers to a derivative with respect to time.

APPARATUS

Bulk Calorimeter

An assembly drawing of the bulk calorimeter is presented in figure 2. The calorimeter is constructed from 16-in. diameter schedule-40 pipe and is mounted in a set of roller supports to facilitate model changes. The calorimeter has three major components: adaptor flange, cooling water spray section, and calorimeter mixing section. The overall length of the apparatus is 4.61 m. Details of the adaptor flange are presented in figure 3. The flange provides an airtight connection between the combustor model and the bulk calorimeter. The rectangular cutout in the flange is designed to accommodate various sizes of combustor models with exit cross sections up to 0.190 by 0.170 m. Several bolt patterns are provided for attaching the combustor model. (See fig. 3.)

Details of the cooling-water spray section are presented in figure 4. Both cooling-water manifolds (fig. 2) supply eight evenly spaced, 2.1-radian, full-cone spray nozzles angled 0.70 radian to the calorimeter center line. Water from the upstream nozzles, which are directed toward the center line at the combustor exit station, quenches combustion. Water from the downstream nozzles provides additional cooling to facilitate measuring the mixture total temperature with thermocouple probes. Metered city water is supplied at a flow rate up to 4.42 liters per second. The quench-water flow rate is adjusted by valves in five parallel lines - one 1.5-in. manually operated gate valve (valve 2) and four remotely operated ball valves (valves 3 to 6). During the current test program, which used only the upstream manifold, valve 2 was set to produce a flow rate of about 0.63 kg/sec, so that with all five valves open (valves 2 to 6) quench-water flow rate was about 1.9 kg/sec. The quench-water flow is turned on and off by valve 1, which is located outside the test cell. (See fig. 4.) Therefore, water flow is unsteady for several seconds as the supply lines fill.

The mixing section provides about 8.5 pipe diameters for the test gas and quench water to become uniformly mixed before the total temperature is measured

at the exit, station B in figure 2. Because of the calorimeter length and the turbulent nature of the flow, the calorimeter walls receive a high heat load. Numerous thermocouples are used to measure the wall temperature at stations labeled A, C, and D in figure 2 to monitor the calorimeter-wall heat loss. These thermocouples are discussed in the section entitled "INSTRUMENTATION."

Direct-Connect Model

The bulk calorimeter was demonstrated using a variation of the direct-connect combustor model described in references 14 and 15. This model has two distinct parts: First, an integrated plug nozzle, swept-strut fuel injector, illustrated in figures 5 and 6; second, a rectangular combustor extension illustrated in figure 7. Figure 5 shows a perspective sketch of the swept-strut fuel-injector section with one sidewall removed. The upstream portion of the centerbody is shaped to form a supersonic nozzle which is designed to produce uniform parallel Mach 1.7 flow upstream of the swept-step and fuel-injector locations. A major modification of the present model from the models discussed in references 14 and 15 is the provision of interchangeable fuel-injector blocks and tail pieces, which are illustrated in figure 6(b). The upstream block includes a rearward facing step and four perpendicular fuel injectors on each side. The contoured tail piece contains two parallel fuel injectors. Coordinates of the tail piece are included in the table in figure 6(b). Details of the perpendicular and parallel fuel injectors are also presented in figure 6(b), and the lateral position of the injectors across the struts are illustrated in figure 6(a).

The combustor model extension, illustrated in figure 7, incorporates diverging top and bottom walls which increase the combustor area ratio from 2.1 to 3.5 (i.e., the ratio of the local combustor cross-sectional area to the cross-sectional area ahead of the step, 0.17h).

INSTRUMENTATION

Instrumentation required for the calorimetric heat balance includes that required for the calorimeter temperature measurements (i.e., mixture total temperature and calorimeter wall temperature); instrumentation to measure the mass-flow rate and temperature of the test gas, combustor fuel, and calorimeter quench water; and instrumentation to measure the heat flux into the combustor model and facility nozzle.

Details of the calorimeter total-temperature probe are presented in figure 8. Figure 8(a) illustrates details of the probe, and figure 8(b) illustrates the location of the 21 total-temperature probes looking upstream at the calorimeter exit. Each probe consists of a commercial, exposed-bead, 0.0032-m diameter, stainless-steel-sheathed, chromel-alumel thermocouple probe installed in a 0.0095-m diameter housing. These housings are capped and have a 0.0025-m diameter inlet orifice on the upstream side and an offset 0.0035-m diameter outlet orifice on the downstream side. The housing protects the thermocouple from flow turbulence and short-duration temperature excursions. The orifice size and location assure high Reynolds number and downflow along the wires to rapidly

heat the housing and wires, thereby reducing both radiative and convective heat loss. The probes are equally spaced circumferentially 0.3 radian apart. Probe number 1 is positioned on the calorimeter center line, and the remaining probes are positioned so that two probes on opposite sides of the calorimeter are located at the radial center of ten equal-area, annular regions. Table I presents a list of the probe radial locations r measured from the calorimeter center line and corresponding area number (area number 1 includes the center line, 10 includes the wall).

The calorimeter-wall temperature is measured by 31 thermocouples. Figure 9(a) illustrates the thermocouple locations, figure 9(b) illustrates construction details of the inside-wall thermocouples, and table II presents a list of the thermocouples and their locations. Twenty-nine of the calorimeter-wall thermocouples are located in the calorimeter mixing section at the stations labeled C and D in figure 2. Stations labeled C have two inside- and two outside-wall thermocouples, and stations D have four inside and four outside thermocouples. (See fig. 9(a).) All wall thermocouples are chromel-alumel and the inside-wall thermocouples screw in as illustrated in figure 9(b). Accuracy and response time for this type of thermocouple was confirmed using a standard wall thermocouple (leads welded to inside surface). Only two thermocouples are located in the cooling-water spray section; one inside-wall thermocouple at each of the stations labeled A in figure 2.

Other measurements required for the calorimetric heat balance include flow rates and temperatures for the following: air, oxygen, and hydrogen to the heater, hydrogen fuel to the combustor model, and quench water. With the exception of the quench water, flow rates are measured with orifice meters. Quench-water flow rate is measured by a turbine meter. The heater total temperature is determined by mass conservation through the facility nozzle throat at the measured heater total pressure.

Other instrumentation for the combustor model measures wall pressure and wall temperature. Because wall pressures are not used in the calorimeter analysis, they are not discussed in this report. One thermocouple used to measure wall temperature is located on the inside wall of the combustor model ahead of the swept step. (See fig. 6(a).) Eight additional thermocouples are located on the outside top wall and side wall of the model extensions, as illustrated in figure 7. The coordinates of these thermocouple locations are presented in table III.

ANALYSIS

Conceptually, the bulk calorimeter quenches the reaction at the exit of the combustion model. Then the temperature of the cooled mixture is measured by thermocouple probes, and the combustion efficiency of the fuel injected into the model is determined by a calorimetric or heat balance of the entire facility-model-calorimeter system. A schematic of the combustion heater, facility nozzle, direct-connect combustor, and the calorimeter is presented in figure 10. The dashed line represents the control volume used to analyze the combustion efficiency of the fuel.

The indicated heat produced by combustion of the fuel is defined as the difference between the heat leaving the control volume and that entering, or the sum of the heat lost to the walls of the apparatus $\dot{Q}_i$ and the change in enthalpy ΔH_j of the constituents of mass flow passing through the control volume. This definition may be expressed as follows:

$$\dot{E}'_p = \sum_i \dot{Q}_i + \sum_j \dot{m}_j \, \Delta H_j \Big|_{T_{in}}^{T_{out}} \tag{1}$$

Wall heat losses considered include the nozzle $\dot{Q}_n$, combustor-model $\dot{Q}_m$, and calorimeter $\dot{Q}_c$.

Flow constituents considered in this analysis are shown by arrows either entering or leaving the control volume in figure 10. Both nitrogen and water vapor pass through the control volume without reacting or changing state, entering at the heater temperature $T_{t,b}$ and leaving at the average calorimeter-exit total temperature $T_{t,p}$. Quench water enters the control volume in the calorimeter at a measured temperature T_q, and leaves in the calorimeter exhaust as steam at $\bar{T}_{t,p}$. Hydrogen fuel, entering the combustor model at ambient temperature, reacts to some extent with oxygen, which entered the control volume at the heater temperature. The combustion products, that is, water and unreacted oxygen and hydrogen, leave the control volume at $\bar{T}_{t,p}$. The mass-flow rates of these combustion products are not known, but they are dependent on combustion efficiency.

The actual heat produced by combustion is dependent on the hydrogen fuel mass-flow rate, the heat of reaction of hydrogen, and combustion efficiency as follows:

$$\dot{E}_p = \dot{m}_f \, \Delta H_R \eta_c \tag{2}$$

Combining equations (1) and (2) produces the following heat balance:

$$\begin{aligned}
\eta_c \dot{m}_f \, \Delta H_R = {} & \dot{m}_{N_2} \, \Delta H_{N_2} \Big|_{T_{t,b}}^{\bar{T}_{t,p}} + \dot{m}_{H_2O} \, \Delta H_{H_2O} \Big|_{T_{t,b}}^{\bar{T}_{t,p}} + \dot{m}_q \left[\Delta H_{H_2O} \Big|_{373\ K}^{\bar{T}_{t,p}} + \Delta H_v \right. \\
& \left. + \Delta H_{H_2O} \Big|_{T_q}^{373\ K} \right] + \dot{m}_{H_2,p} \, \Delta H_{H_2} \Big|_{T_f}^{\bar{T}_{t,p}} + \dot{m}_{O_2,p} \, \Delta H_{O_2} \Big|_{T_{t,b}}^{\bar{T}_{t,p}} \\
& + \dot{m}_{H_2O,p} \left[H_{H_2O,\bar{T}_{t,p}} - \frac{M_{O_2}}{M_{H_2O}} H_{O_2,T_{t,b}} - \frac{M_{H_2}}{M_{H_2O}} H_{H_2,T_f} \right] \\
& + \dot{Q}_n + \dot{Q}_m + \dot{Q}_c
\end{aligned} \tag{3}$$

where the mass flow of the combustion products are

$$\dot{m}_{H_2,p} = (1 - \eta_c)\dot{m}_f \tag{4}$$

$$\dot{m}_{O_2,p} = \dot{m}_{O_2} - \eta_c \dot{m}_f \left(\frac{2\mu_{O_2}}{\mu_{H_2}}\right) \tag{5}$$

$$\dot{m}_{H_2O,p} = \eta_c \dot{m}_f \left(\frac{\mu_{H_2O}}{\mu_{H_2}}\right) \tag{6}$$

Equations (3) to (6) are solved, using an iterative procedure, to determine the combustion efficiency of the fuel.

Exit Temperature

The bulk- or mass-weighted calorimeter exit temperature is estimated using an area-weighted temperature. Because of the locations of the temperature probes, the area-weighted temperature is obtained by the arithmetic average of all the total-temperature probe readings except the center-line probe (i = 1). Therefore,

$$\bar{T}_{t,p} = \frac{1}{20} \sum_{i=2}^{21} (T_{t,p})_i \tag{7}$$

(Note in table I that the center-line probe is one of three probes located in area number 1.)

Calorimeter-Wall Heat Loss

Heat lost to the calorimeter wall $\dot{Q}_c$ is determined considering the heat capacity of the calorimeter. Expressed differentially, heat capacity is

$$\dot{Q}_c = cm\,\dot{\bar{T}}_c \tag{8}$$

where c, the specific heat of the wall (from ref. 20), is

$$c = 0.4672\bar{T}_c + 329.12 \tag{9}$$

m is the wall mass, and $\dot{\bar{T}}_c$ is the time derivative of the average calorimeter-wall temperature. The average temperature of the calorimeter wall, assuming a

linear temperature distribution from the inside to outside, is obtained by averaging the twenty-eight inside- and outside-wall temperature measurements. (Experimental results indicate that the average wall temperature in the water-spray section and the mixing section are approximately equal.) The time derivative of the average temperature is determined by using a linear-regression analysis of the average calorimeter-wall temperature T_C over a two-second interval to smooth the temperature fluctuations. For constant steady-state heat flux with no backwall radiation, the semi-infinite slab theory (ref. 21) predicts the difference between the true mass-average temperature and the linear average of inside- and outside-wall temperatures T_{LA}. This theory is given by

$$\bar{T}_C - T_{LA} = -1.05 \times 10^{-5} \dot{Q}_C \tag{10}$$

Equations (8) to (10) are solved in an iterative fashion to determine Q_C from the average of the measured inside- and outside-wall temperatures.

The calorimetric analysis requires determination of the heat lost to the walls of the nozzle and combustor model. The nature of this combustor model suggests separate analysis methods for the integral-plug-nozzle swept-strut model and the extension ducts. Heat lost to the former is referred to as nozzle heat loss $\dot{Q}_n$ and heat lost to the latter is referred to as model heat loss $\dot{Q}_m$.

Nozzle Heat Loss

Because of the complex geometry, the combined active heat-sink cooling, and the limited nozzle wall temperature instrumentation, the nozzle heat loss is determined by using the turbulent boundary-layer program discussed in reference 22 with the assumption of uniform wall temperature equal to that which was measured. This empirical analysis shows that

$$Q_n = 0.000313 p_b^{0.8} T_t^{0.1} (T_t - T_w) \tag{11}$$

which, from necessity, neglects any heat loss to the nozzle-strut section from fuel combustion. The effect of this instrumentation limitation on the overall analysis is discussed subsequently.

Combustor-Model Heat Loss

Heat loss to the walls of the combustor-model extension $\dot{Q}_m$ is estimated by using an analysis similar to that used for the calorimeter heat loss. $\dot{Q}_m$ is estimated by comparing the average outside-wall temperature with a correlation of the results of semi-infinite slab heating analysis (ref. 21). With the assumption of no back-wall radiation, the semi-infinite slab analysis predicts that for a constant applied heat flux the temperature rise of the outside surface is proportional to the heat flux. For the 1.27-cm-thick wall of the combustor model extension, after a short transition time (2 to 6 sec),

$$\dot{Q}_m = 1.4015 \times 10^4 \, \dot{\bar{T}}_m A_m \tag{12}$$

where $\bar{T}_m$ is the average outside-wall temperature. The instantaneous value of $\dot{\bar{T}}_m$ is estimated using a linear-regression analysis of the average model temperature over a 2-second interval to smooth the temperature fluctuations.

Tare

A method of checking the accuracy of the heat balance is to evaluate equation (1) for the condition with no fuel injection to the combustor model, that is, where the heat-produced E_p is zero. The fractional error of the heat-balance analysis is the ratio of the indicated heat produced E_p' to the total energy of the test gas

$$t = E_p'/E_{TG} \tag{13}$$

where

$$E_{TG} = \dot{m}_{air} \, \Delta H_{air} \Big|_{T_{air}}^{T_{t,b}} + \dot{m}_{H_2} \, \Delta H_{H_2} \Big|_{T_{H_2}}^{T_{t,b}} + \dot{m}_{O_2} \, \Delta H_{O_2} \Big|_{T_{O_2}}^{T_{t,b}} \tag{14}$$

and E_p is calculated using equation (1), with $\dot{m}_f = 0$. If the measured tare values are significant, they are included in the combustion-efficiency analysis as follows:

$$\eta_c' = \frac{\eta_c - t(E_{TG}/E_F)}{1 + t} \tag{15}$$

DEMONSTRATION OF THE BULK CALORIMETER

The bulk calorimeter was demonstrated using an ongoing direct-connect combustor test. The objective of the demonstration was to observe the behavior of the calorimeter calculations in the test environment, check the accuracy and repeatability of the calorimetric balance, determine if reaction in the flow leaving the combustor is quenched, and demonstrate the potential of the calorimeter as a research tool. Results of the calorimeter analysis are presented in this section, including results of the tare and combustion-efficiency analysis.

Typical Calorimeter Response

Figures 11 and 12 present experimental measurements, calculated heat losses, and combustion efficiency for a typical calorimeter test. These results are presented to demonstrate the dynamic characteristics of the data and the resulting limitations of the calorimetric analysis. Figure 11(a) illustrates variation with time of the test conditions and the calculated combustion efficiency. Arrows located on the abscissa of this plot denote test events affecting the measurements. The arrow labeled $\dot{m}_b$ indicates the time when the heater reaches steady-state operation, at about $\tau = 2$ seconds. This run incorporates a two-step fuel-injection schedule. The arrow labeled ϕ_1 indicates the time when upstream (perpendicular) fuel injection starts, at about 3 seconds; the arrow labeled ϕ_2 indicates the time when downstream (parallel) fuel injection starts, at about 6 seconds. The calorimeter water supply is turned on automatically 0.5 second after the heater propellant supply valves open, but nearly 5 seconds are required to reach steady quench-water flow. Thus, the arrow labeled $\dot{m}_q$ which indicates the time quench water starts, is located on the abscissa at about 4.5 seconds.

The analysis program is used to calculate tare when the model fuel flow is zero, and combustion efficiency when the model fuel flow is greater than zero. Calculated combustion efficiency results are presented in figure 11(a). For the first fuel schedule condition, the calculated combustion-efficiency results range from 1.2 to 0.97. When downstream fuel injection is added the combustion efficiency drops to 0.82 then returns to about 0.93.

Experimental measurements and calculated wall heat losses used in the calorimetric analysis of combustion efficiency, which are presented in figures 11(b) to 11(d), provide some insight into the unsteady character of the calculated combustion efficiency. These results demonstrate the transient nature of all the variables in the analysis. Figure 11(b) illustrates the transient characteristics of the nozzle wall temperature and nozzle heat loss. The nozzle inside-wall temperature increases from ambient to about 480 K at the end of the run. Therefore, for nearly constant heater total pressure and temperature, the heat flux decreases as the wall temperature increases. For this test, the total heat of the test gas is about 4.43 MJ/sec, so the total nozzle heat loss decreases with time from about 12 to 7 percent of that in the test gas. Toward the end of the run, the total heat loss to the nozzle wall is about 3 percent of the total heat of reaction available in the fuel (10.0 MJ/sec).

Figure 11(c) illustrates the transient characteristics of the combustor-model average outside-wall temperature and the calculated model heat loss. The average model temperature has a nearly constant slope after an initial 6-second transient. For this case, the start-up transient extends well into the first fuel schedule. Downstream injection is started after the transient part of the curve, but has negligible effect on the wall heat loss because the parallel fuel ϕ_2 burns away from the model wall adding little if any heat to the combustor

model. The combustor-model heat loss, calculated using equation (12), increases during the transitional part of the temperature curve, then is nearly constant at about 0.63 MJ/sec, or 6 percent of the total heat of reaction available in the fuel.

Figure 11(c) demonstrates two limitations of the analytical procedure. First, during the transient part of the temperature curve, the model heat loss is grossly underpredicted due to the slow response of the outside-wall temperature. When the test-gas temperature and pressure are nearly constant through the run, the relatively cool wall temperature early in the run should result in higher heat flux, as observed in figure 11(b) for the nozzle or as sketched by the dashed line in figure 11(c). Second, the curve-fit routine uses data over a 2-second interval to determine the first derivative of temperature for equation (12). Therefore, the combustor-model heat loss calculated during the transitional parts of the temperature curve, or 1 second before or after such a transition (including the end of the test) is unrealistic. Other test results have shown that if the fuel injection is delayed until after 6 seconds, the transition from the linear curve representing the heat flux with no fuel injection to the linear curve with fuel injection requires only 1 to 2 seconds.

Figure 11(d) illustrates the general transient characteristics of the calorimeter by presenting two typical wall temperatures, the calculated calorimeter-wall heat loss, and the average total temperature of the mixture at the calorimeter exit. The two calorimeter temperatures presented are inside- and outside-wall temperatures at the first station in the mixing section. Test events, denoted by arrows on the abscissa, are reflected in the data. For example, step increases in the fuel mass flow, denoted ϕ_1 and ϕ_2, produce rapid (about 1-second delay) rises in the inside-wall temperature. The initial overshoot in the calorimeter heat loss results from the hot combustor-model exhaust entering the calorimeter before the quench water is up to full flow. As with the combustor-model heat loss, a linear-regression analysis spanning 2 seconds is used in determining the first derivative of average wall temperature used in calculating the calorimeter-wall heat loss. Thus, any step-like change in the applied heat flux influences calculations 1 second before or after the change. After the initial calorimeter transients, the wall heat loss represents about 10 to 14 percent of the total heat of reaction available in the fuel.

Figure 12 presents the calorimeter-exit total-temperature profile for this typical test. The total-temperature profile at $\tau = 8$ seconds is fairly uniform over the calorimeter exit except for the thermal boundary layer at the wall. The profile exhibits a slightly lower temperature near the center line, which is accentuated for tests which have a higher ratio of quench water to total test-gas mass flow. This indicates that the quench water is reaching the combustor center line. Because the two data points presented at the same radius are located on opposite sides of the calorimeter, these results demonstrate that the temperature is uniform circumferentially. Pitot and static pressure surveys at the calorimeter exit also show that the mass flow per unit area is relatively uniform, and thus the area-averaged total temperature used in the analysis closely approximates the mass-averaged total temperature. For a typical test, the ratio of area-weighted to the mass-weighted total temperature was determined to be 0.997.

These typical results demonstrate the operational characteristics of the calorimeter and illustrate some limitations which need to be considered in the analysis. Calculated combustion efficiency is not realistic during heat-flux transients. The large start-up transient requires about 5 or 6 seconds; fuel-schedule transients during the run require up to 2 seconds. The key to determining the extent of these transients is in the individual measured-wall temperatures. For the results presented in figure 11, the calculated combustion efficiency is not realistic at τ = 3 and 4 seconds because of the start-up transients; at 5, 6, and 7 seconds because of the transient associated with fuel-flow schedule change (ϕ_2), or at 13 seconds because of the run shutdown. The data points at these times are shaded on figure 11(a). For this run, the only reliable combustion-efficiency results are for the second fuel schedule, i.e., both upstream and downstream injection. Although only one fuel schedule was successfully analyzed for the run demonstrated, it is apparent that with careful timing 2 fuel schedules can be analyzed during one 12- to 14-second run. In the remaining discussion, test conditions and combustion efficiencies for the credible results are averaged to obtain a single time-averaged value for each run and/or fuel schedule.

Experimental Results

An evaluation of the bulk calorimeter was made by measuring the tare and combustion efficiency for a series of runs using the fuel injectors illustrated in figure 6. Twenty-four runs were made with this configuration: ten with no fuel injection and fourteen with fuel injection. Most of the runs without fuel injection were made at heater pressure and temperature spanning the test conditions used with fuel injection. However, three of the runs were made at higher pressure to simulate the total heat flux of the fuel-injection tests. Runs with fuel injection were made at two nominal test conditions simulating the combustor-entrance total temperature at flight Mach numbers of 5 and 6, with a wide range of fuel schedules covering total-equivalence ratios from 0.3 to 0.95. Test conditions and calorimeter results are summarized in tables IV and V. Discussion of these results is presented as follows: first, selected results are used to demonstrate the fractional error of the heat balance, i.e., tare. Next, the calorimeter quenching is discussed. Finally, typical results are presented to demonstrate the consistency of the results and the potential of the calorimetric analysis to make rapid evaluation of combustion performance.

Tare.- Values of measured tare ranged from -0.0030 to 0.0698, as illustrated in table IV. An analysis was performed to determine if these tare values were dependent on any of the test conditions or measurements used in the calorimetric balance. This analysis identified the average total temperature at the calorimeter exit $\bar{T}_{t,p}$ as the only variable on which tare is dependent. This dependence is illustrated graphically in figure 13, where all the tare results are presented as a function of $\bar{T}_{t,p}$ and are correlated by

$$t = 0.0656 - 0.0000814\bar{T}_{t,p} \tag{16}$$

Although other correlations are suggested by the limited data presented, the correlation selected was observed in other preliminary tests and has a theoretical basis. Eight of the ten values fall within ±1 percent of this correlation. There is no apparent explanation for the other two values, thus they represent the current state of possible but infrequent random error in the heat-balance analysis. The data trend expressed by equation (16) illustrates a two-percent error in the calorimetric balance when the calorimeter total temperature is about 550 K. As the total temperature is increased, the error decreases so that at about 830 K there is no error in the analysis. This trend is qualitatively the same as that produced by radiation error in the thermocouple readings. Radiation error produces a low indicated temperature. The magnitude of the error increases with temperature. Thus, at higher probe temperature, the radiation error (which is not accounted for in the analysis) causes a decreasing trend in the indicated energy produced E_p. Because of these tare analysis results, the quench water was preset to produce $\bar{T}_{t,p} \approx 830$ K in the remaining calorimeter runs. However, because it proved difficult to produce the desired calorimeter-exit total temperature, the combustion-efficiency results were tare corrected using equations (13) and (16). Both uncorrected and corrected combustion-efficiency results are listed in table V.

Quenching.- It is difficult to demonstrate calorimeter quenching without an independent measure of the local combustion efficiency. Repeatability of measurements and the range of measured combustion efficiency give an indication that for certain conditions quenching is likely. Repeating a run with several different flow rates of quench water can demonstrate failure to quench, but repeatable readings do not prove that quenching occurred. In the current test series, one fuel schedule which had a low indicated combustion efficiency was repeated with different quench-water flow rates to determine if the quench-water flow rates affect the quenching or the indicated combustion efficiency. Figure 14 presents the calculated combustion efficiency for three runs which have quench-water flow rates from 0.47 to 1.58 liters per second and calorimeter-exit average total temperatures from 618 to 1057 K, respectively. These results show that about half the hydrogen passed through the calorimeter without reacting, and that variations in neither quench-water flow rate nor calorimeter total temperature (within range tested) alter the indicated combustion efficiency. Repeatability of these combustion-efficiency measurements are ±3 percent.

Two measures of the exit average combustion efficiency are available from measurements independent of the calorimeter: One-dimensional analysis (ref. 9) of measured wall pressure and heat flux and integrations of gas-sample and pitot-pressure measurements. (See ref. 17.) The one-dimensional analysis of the combustor performance, which has not been completed, will be discussed in a subsequent report. Results from the one-dimensional analysis of the three tests illustrated in figure 14 have been obtained, and agree with the calorimeter results within ±5 percent, which indicates that combustion has been quenched by the calorimeter for this test-gas fuel-schedule condition.

Gas-sample and pitot-pressure surveys were obtained for two test conditions to provide an independent measure of both mixing and combustion efficiencies for comparison with the calorimeter results. Mixing efficiency, defined as that fraction of the total fuel which would burn if complete chemical reaction occur-

red at every point in the flow without additional mixing, is an upper bound on combustion efficiency at the axial station in the flow. Although mixing efficiency can be determined accurately (±5 percent) from the survey data, combustion efficiency can only be estimated (±10 percent) because the sample probes complete reaction of the samples as they are acquired. Combustion efficiency is inferred by forcing the integrated mass-flow rates to equal the metered mass-flow rates. A semi-empirical model of local combustion efficiency with local equivalence ratio is used in this technique as discussed in reference 12. Mixing- and combustion-efficiency results, obtained by gas samples, are compared in figure 15 with the combustion-efficiency results obtained with the calorimeter. For both test-condition comparisons, combustion efficiency determined by the calorimeter is less than the mixing efficiency, which indicates that the calorimeter quenched combustion at or near the combustor-model exit.

Comparison of combustion efficiency at the low test-gas total temperature are good (±5 percent), which suggests that the flow is quenched and that the heat balance is accurate. The comparison of the high test-gas total-temperature (1670 K) results are not as good, which suggests that either the calorimeter did not completely quench combustion for this case or that the estimated combustion efficiency from gas samples is in error. Additional independent measures of combustion efficiency, such as the one-dimensional analysis mentioned previously, are required to verify the quenching.

Combustor performance.- This section presents an analysis of the combustion-efficiency results for the direct-connect combustor-model configuration tested. This analysis is presented to illustrate the potential of the calorimeter and to illustrate the consistency of the calorimeter measurements of combustion efficiency.

For this model and injector geometry, test variables expected to influence η_c are the test-gas total temperature and pressure and the fuel-equivalence ratio of the upstream and downstream injectors. Values of these parameters for each test are listed in table V. Although the sample population is less than ideal, a linear-regression analysis was performed to derive a correlation of the measured combustion efficiency with the aforementioned test variables. Because the test-gas temperature and pressure were not varied independently in the runs, the effect of either variable on combustion efficiency cannot be separated from the effect of the other. Temperature was chosen for the correlation because it has a larger span (range from 850 to 1450 K). Details of the method of analysis are illustrated by considering the dependence of η_c on test-gas total temperature.

All the combustion-efficiency results obtained in this study (see table V) are presented in figure 16 as a function of the test-gas total temperature. Generally, the test conditions simulated either Mach 5 or Mach 6 flight enthalpy. These results were also separated into two groups by fuel schedule. Low-combustion efficiency (0.45 to 0.55) was observed for all runs which had only parallel injection. High-combustion efficiency was observed for runs which had any upstream or perpendicular injection. Although the data within these two groups have a diverse range of fuel schedules, the linear-regression analysis of

both data groups indicates that combustion efficiency is statistically dependent on the test-gas total temperature. Linear-regression analysis results illustrated by the dashed lines in figure 16 are

$$\eta_c' = 0.64 + 0.000181T_{t,b} (R = 0.77) \tag{17}$$

$$\eta_c' = 0.264 + 0.000191T_{t,b} (R = 0.82) \tag{18}$$

for the data groups with and without upstream fuel injection, respectively. Thus, for this combustor model, with a fixed fuel schedule, increasing the test-gas temperature increases the combustion efficiency.

Linear-regression analysis also indicates that the combustion efficiency is not dependent on the value of ϕ_1 (as long as ϕ_1 is greater than 0.2), but combustion efficiency is dependent on ϕ_2 and is conditionally dependent on the total fuel equivalence ratio $(\phi_1 + \phi_2)$. For this direct-connect combustor model, it was found that a useful parameter for correlating the combustion efficiency is the fuel-schedule parameter $S_F = \phi_2/(\phi_1 + \phi_2)$, which represents the fraction of the total fuel injected from the parallel fuel injectors (ϕ_2). Figure 17 shows that all the tare-corrected combustion-efficiency results can be correlated within ±10 percent by

$$N = (0.640 + 0.000181T_{t,b})\left(1.020 + 0.041S_F - 0.480S_F^2\right) \tag{19}$$

which accounts for both the fuel schedule and facility total temperature. This correlation shows that, for this combustor model, upstream fuel injection is required for good combustion and that downstream fuel injection lowers the combustion efficiency at the duct exit. This correlation is presented to demonstrate the potential of the calorimeter for rapid analysis of combustor performance and to demonstrate the consistency of the results of the calorimetric analysis. Each point is acquired with one test run and analyzed within a few seconds after the run. On the other hand, the gas-sample analysis requires from 6 to 8 individual runs plus merging of data from two computers. The one-dimensional analysis requires only one run but is not an easy analysis tool when the flow contains shock waves and/or separation regions. The calorimeter analysis overcomes both these deficiencies.

CONCLUDING REMARKS

Details of a bulk calorimeter and results from a shakedown and evaluation test are presented. These results demonstrate that the calorimeter quenches the combustion at the exit of the direct-connect, hydrogen-fueled, scramjet combustor model, and provide measurements of the combustor heat flow required to perform a heat-balance analysis of the fuel combustion efficiency. Details presented include the bulk-calorimeter hardware and instrumentation; the heat balance analysis which provides a measure of combustion efficiency when the fuel

is on, or a measure of the fractional error in the analysis when fuel is off; and a demonstration of the quasi steady-state operation of the calorimeter heat-balance analysis.

The bulk calorimeter was demonstrated in tests with a Mach 1.7 hydrogen-fueled, direct-connect, swept-strut combustor model. Typical results presented show that the calorimeter analysis is quasi steady state, in that the various heat-balance terms (i.e., wall heat loss, heater temperature, etc.) do not reach steady state during the run. The analysis method is designed for this quasi steady-state condition, and provides accurate solutions except during severe transients. Tare analysis (with no fuel flow) demonstrates that the heat-balance analysis is accurate within ±2 percent and that the error in the heat balance is qualitatively similar to radiation errors of the calorimeter total-temperature probe. Applying this tare correction, the heat-balance analysis is accurate within ±1 percent.

Calorimeter quenching was demonstrated by three methods. Measured combustion efficiency ranged from 0.45 to 0.95 with test variables in an expected manner, which indicated that the calorimeter rapidly quenched the combustion. Repeatability of calculated combustion efficiency is on the order of ±3 percent even when the quench-water flow rate is varied. Comparison of the calculated combustion efficiency with values obtained by other methods demonstrates that the calorimeter results agree within the known accuracy of the other methods.

The shakedown test demonstrated that by using the bulk calorimeter it is possible to obtain an accurate (±3 percent) determination of the combustion efficiency for two fuel conditions during one 15-second test, and to have the results available within a few seconds of the completion of the run.

Langley Research Center
National Aeronautics and Space Administration
Hampton, VA 23665
November 21, 1980

REFERENCES

1. Becker, John V.: Prospects for Actively Cooled Hypersonic Transports. Astronaut. & Aeronaut., vol 9, no. 8, Aug. 1971, pp. 32-39.

2. Henry, J. R.; and McLellan, C. H.: Air-Breathing Launch Vehicle for Earth-Orbit Shuttle - New Technology and Development Approach. J. Aircr., vol. 8, no. 5, May 1971, pp. 381-387.

3. Henry, John R.; and Anderson, Griffin Y.: Design Considerations for the Airframe-Integrated Scramjet. NASA TM X-2895, 1973.

4. Anderson, Griffin Y.: An Examination of Injector/Combustor Design Effects on Scramjet Performance. NASA paper presented at the 2nd International Symposium on Air Breathing Engines (Sheffield, England), March 25-29, 1974.

5. Russin, William Roger: Performance of a Hydrogen Burner To Simulate Air Entering Scramjet Combustors. NASA TN D-7567, 1974.

6. Guy, Robert W.; and Mackley, Ernest A.: Initial Wind Tunnel Tests at Mach 4 and 7 of a Hydrogen-Burning, Airframe-Integrated Scramjet. NASA paper presented at the 4th International Symposium on Air Breathing Engines (Lake Buena Vista, Fla.), April 1-6, 1979.

7. Russin, Wm. Roger: The Effect of Initial Flow Nonuniformity on Second-Stage Fuel Injection and Combustion in a Supersonic Duct. NASA TM X-72667, 1975.

8. Rogers, R. C.; and Eggers, J. M.: Supersonic Combustion of Hydrogen Injected Perpendicular to a Ducted Vitiated Airstream. AIAA Paper No. 73-1322, Nov. 1973.

9. Eggers, James M.; Reagon, Patricia G.; and Gooderum, Paul B.: Combustion of Hydrogen in a Two-Dimensional Duct With Step Fuel Injectors. NASA TP-1159, 1978.

10. McClinton, Charles R.: Interaction Between Step Fuel Injectors on Opposite Walls in a Supersonic Combustor Model. NASA TP-1174, 1978.

11. Anderson, Griffin Y.; and Gooderum, Paul B.: Exploratory Tests of Two Strut Fuel Injectors for Supersonic Combustion. NASA TN D-7581, 1974.

12. McClinton, C. R.; and Gooderum, P. B.: Direct-Connect Test of a Hydrogen-Fueled Three-Strut Injector for an Integrated Modular Scramjet Engine. 14th JANNAF Combustion Meeting, Volume II, T. W. Christian, ed., CPIA Publ. 292 (Contract N00017-72-C-4401), Appl. Phys. Lab., Johns Hopkins Univ., Dec. 1977, pp. 489-505.

13. Rogers, R. C.: Influence of Fuel Temperature on Supersonic Mixing and Combustion of Hydrogen. AIAA Paper 77-17, Jan. 1977.

14. Anderson, Griffin Y.; Reagon, Patricia G.; Gooderum, Paul B.; and Russin, W. Roger: Experimental Investigation of a Swept-Strut Fuel-Injector Concept for Scramjet Application. NASA TN D-8454, 1977.

15. Northam, G. B.; Trexler, C. A.; and Anderson, G. Y.: Characterization of a Swept-Strut Hydrogen Fuel-Injector for Scramjet Applications. 15th JANNAF Combustion Meeting, Volume III, T. W. Christian, ed., CPIA Publ. 297, (Contract N00024-78-C-5384), Appl. Phys. Lab., Johns Hopkins Univ., Feb. 1979, pp. 393-410.

16. McClinton, Charles R.: Autoignition of Hydrogen Injected Transverse to a Supersonic Airstream. AIAA Paper 79-1239, June 1979.

17. Eggers, James M.: Composition Surveys of Test Gas Produced by a Hydrogen-Oxygen-Air Burner. NASA TM X-71964, 1974.

18. Reed, R. A.; and Slack, M. W.: Infrared Measurements of a Scramjet Exhaust. NASA CR-3242, 1980.

19. Billig, F. S.; Orth, R. C.; and Funk, J. A.: Direct-Connect Tests of a Hydrogen-Fueled Supersonic Combustor. NASA CR-1904, 1971.

20. Baumeister, Theodore, ed.: Marks' Mechanical Engineers' Handbook. Sixth ed., McGraw-Hill Book Co, Inc., 1958.

21. Drummond, John Philip: A Method for Improving the Accuracy in Phase Change Heat Transfer Data Through Increased Precision in Thermophysical Property Determinations. M. Eng. in Mech. Eng. Thesis, Old Dominion Univ., 1975.

22. Pinckney, S. Z.: Turbulent Heat-Transfer Prediction Method for Application to Scramjet Engines. NASA TN D-7810, 1974.

TABLE I.- CALORIMETER TEMPERATURE PROBES

Number	Area	r, m	θ, rad
1	1, ¢	0	0
2	10	.188	.30
3	1	.043	.60
4	9	.178	.90
5	2	.074	1.20
6	8	.168	1.50
7	3	.097	1.80
8	7	.155	2.09
9	4	.114	2.39
10	6	.142	2.69
11	5	.130	2.99
12	1	.043	3.29
13	10	.188	3.59
14	2	.074	3.89
15	9	.178	4.19
16	3	.097	4.49
17	8	.168	4.79
18	4	.114	5.08
19	7	.155	5.39
20	5	.130	5.68
21	6	.142	5.98

TABLE II.- CALORIMETER-WALL THERMOCOUPLE LOCATIONS

Number	x_c, m	θ, rad	Location
1	1.22	0	Inside wall
2		1.57	Outside wall
3		3.14	Inside wall
4		4.71	Outside wall
5	1.83	0	Outside wall
6		.79	Inside wall
7		1.57	Outside wall
8		2.36	Inside wall
9		3.14	Outside wall
10		3.93	Inside wall
11		4.71	Outside wall
12		5.50	Inside wall
13	2.44	0	Inside wall
14		1.57	Outside wall
15		3.14	Inside wall
16		4.71	Outside wall
17	3.05	0	Outside wall
18		.79	Inside wall
19		1.57	Outside wall
20		2.36	Inside wall
21		3.14	Outside wall
22		3.93	Inside wall
23		4.71	Outside wall
24		5.50	Inside wall
25	3.66	0	Inside wall
26		1.57	Outside wall
27		3.14	Inside wall
28		4.71	Outside wall
29		3.14	Inside wall
30	.30	.79	Inside wall
31	.61	.79	Inside wall

TABLE III.- MODEL OUTSIDE-WALL THERMOCOUPLE LOCATIONS

Number	x_m, m	Location
1	0.076	Top wall
2	.076	Side wall
3	.229	Side wall
4	.229	Top wall
5	.381	Top wall
6	.381	Side wall
7	.533	Side wall
8	.533	Top wall

TABLE IV.- SUMMARY OF TEST CONDITIONS AND RESULTS FOR TARE ANALYSIS

Test	$T_{t,b}$, K	$P_{t,b}$, MPa	$\bar{T}_{t,p}$, K	$\dot{E}_{TG}$, MJ/sec	Tare
1	963	1.14	731	5.75	0.0107
2	1427	.66	786	4.47	.0020
3	1186	.71	719	4.14	-.0003
4	1067	.74	659	3.99	.0062
5	1441	.65	811	4.43	.0698
6	1558	.70	557	5.08	.0303
7	1549	.69	833	5.00	.0024
8	967	1.35	763	6.73	-.0030
9	1027	.74	656	3.86	.0191
10	1424	.64	750	4.32	.0440

TABLE V.- SUMMARY OF TEST CONDITIONS AND RESULTS FOR

COMBUSTION-EFFICIENCY ANALYSIS

Test	$T_{t,b}$, K	$p_{t,b}$, MPa	ϕ_1	ϕ_2	$\bar{T}_{t,p}$, K	$\dot{E}_F$, MJ/sec	$\bar{\eta}_c$	$\bar{\eta}'_c$
1	1422	0.65	0	0.296	1057	4.38	0.496	0.514
2	1428	.66	0	.290	808	4.36	.510	.508
3	1426	.66	0	.291	618	4.35	.581	.564
4	1044	.74	0	.277	686	4.92	.468	.456
5	1433	.66	.451	0	718	4.33	.958	.949
6	1438	.65	.663	0	875	6.21	.915	.918
7	1072	.74	.452	0	791	5.37	.881	.878
8	846	.72	.619	.171	1004	6.87	.800	.814
9	923	.75	.456	.125	1041	6.81	.821	.838
10	1025	.73	.205	.124	795	3.95	.789	.786
11	1048	.74	.432	.124	832	6.82	.765	.765
12	1065	.74	.456	.128	856	6.91	.813	.815
13	1440	.66	.341	.291	828	6.01	.888	.888
14	1434	.66	.669	.286	986	9.14	.850	.862

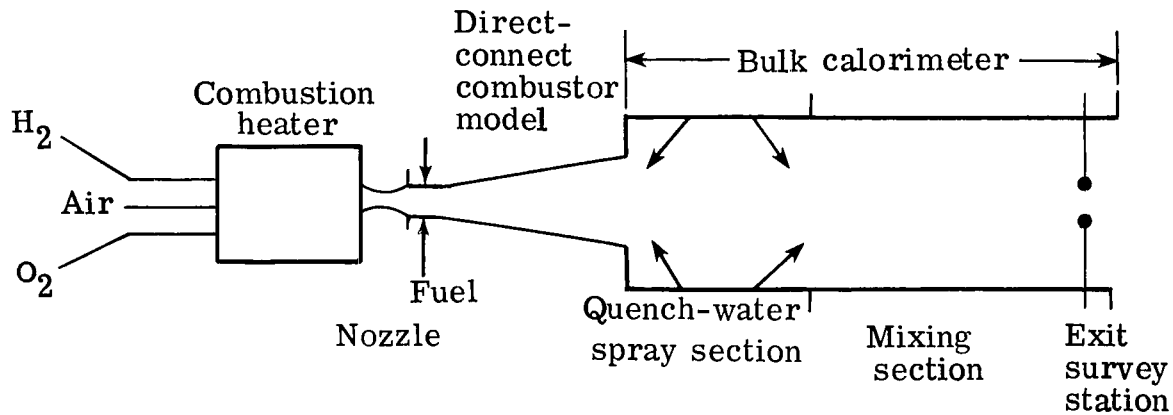

Figure 1.- Schematic of apparatus.

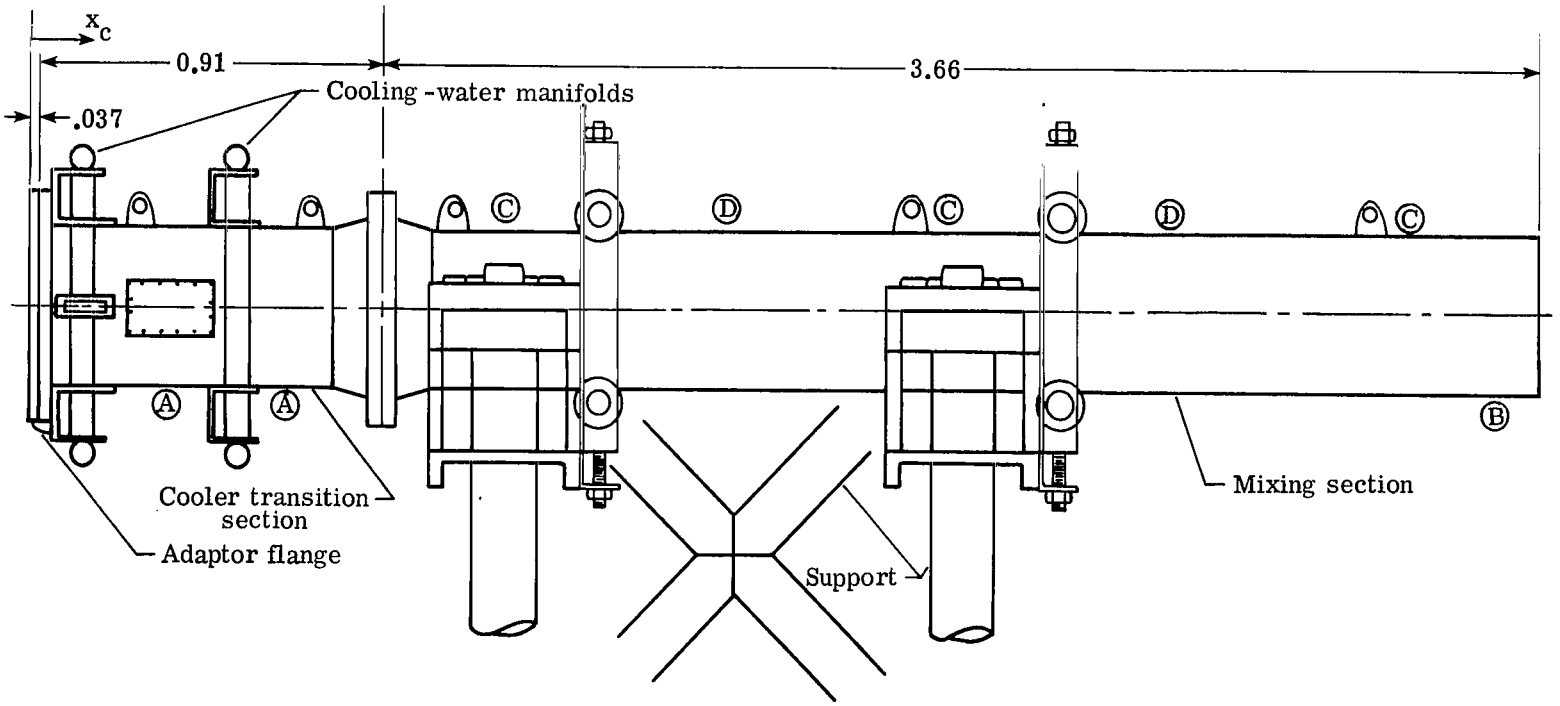

Figure 2.- Bulk calorimeter apparatus. All dimensions are in meters.

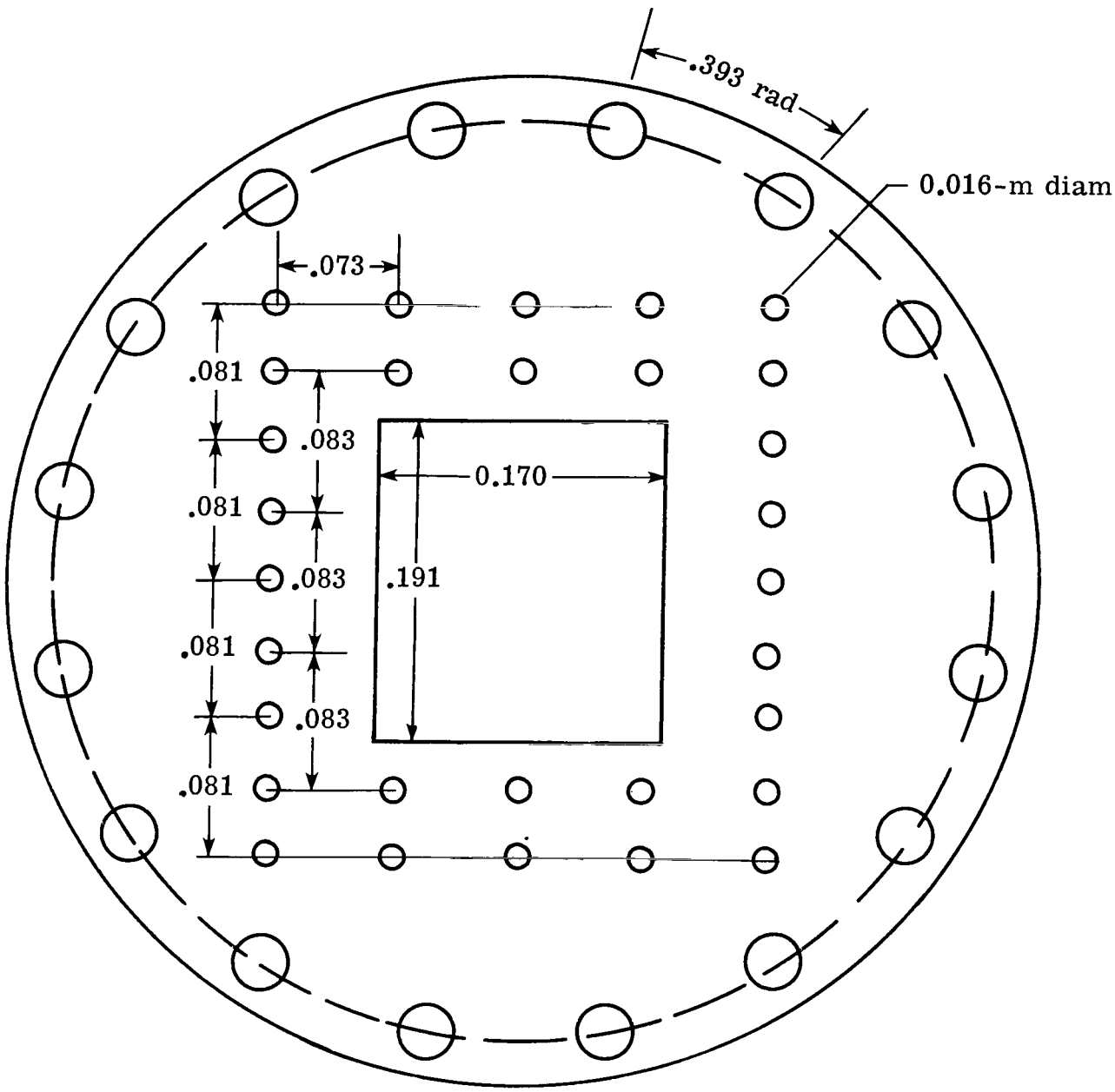

Figure 3.- Details of adaptor flange. All dimensions are in meters.

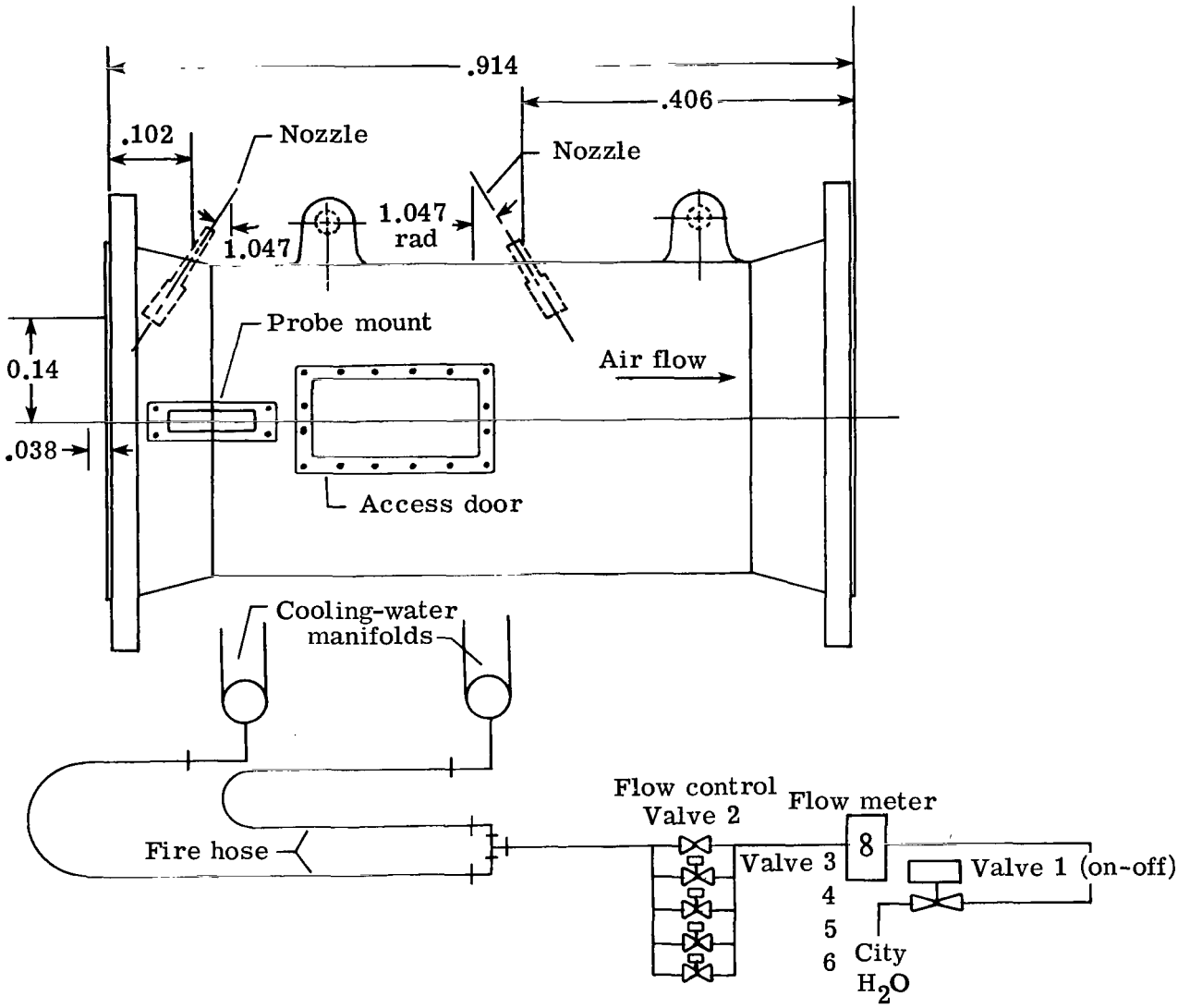

Figure 4.- Cooler transition-section details. All dimensions are in meters.

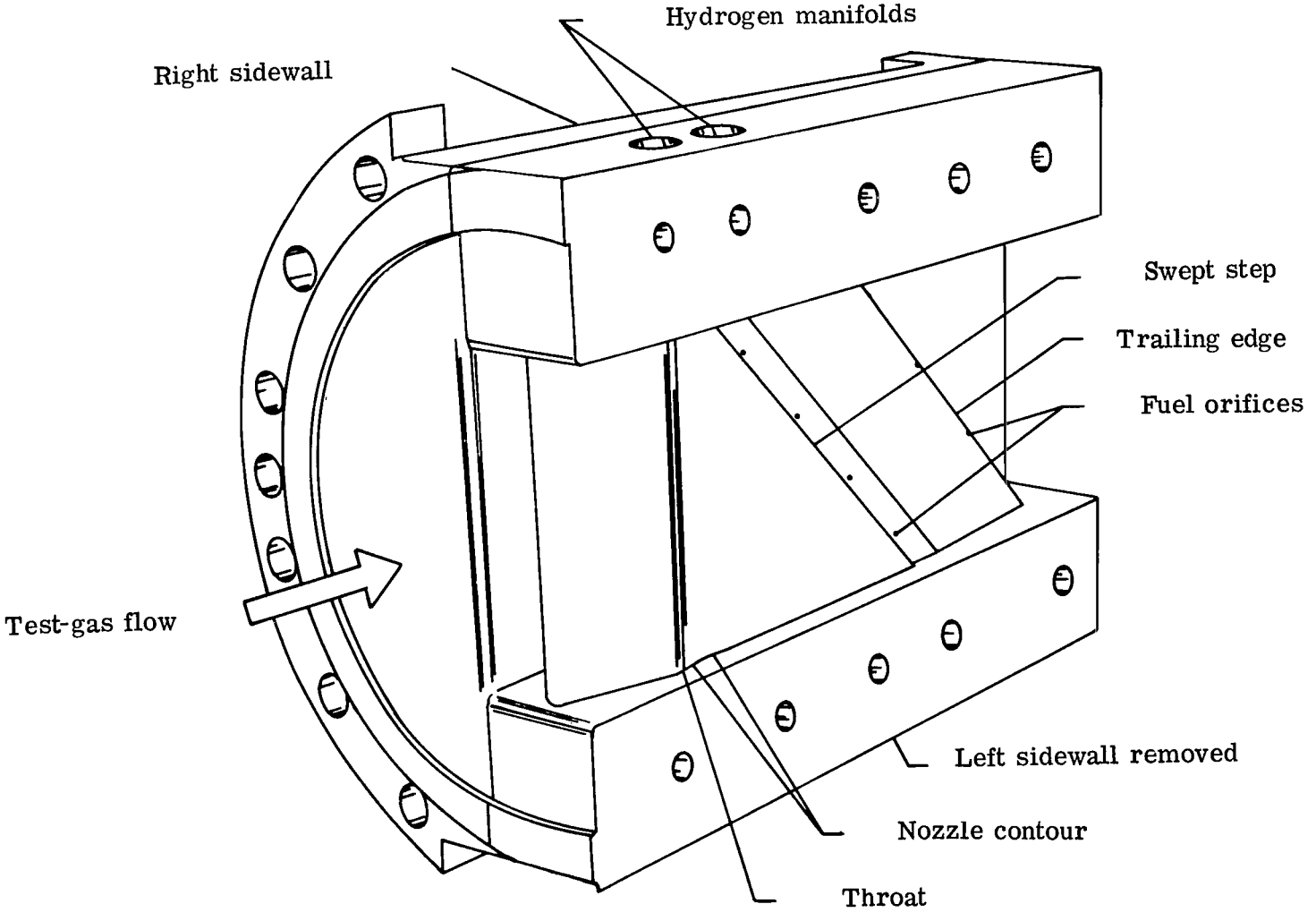

Figure 5.- Perspective view of swept-strut fuel injector.

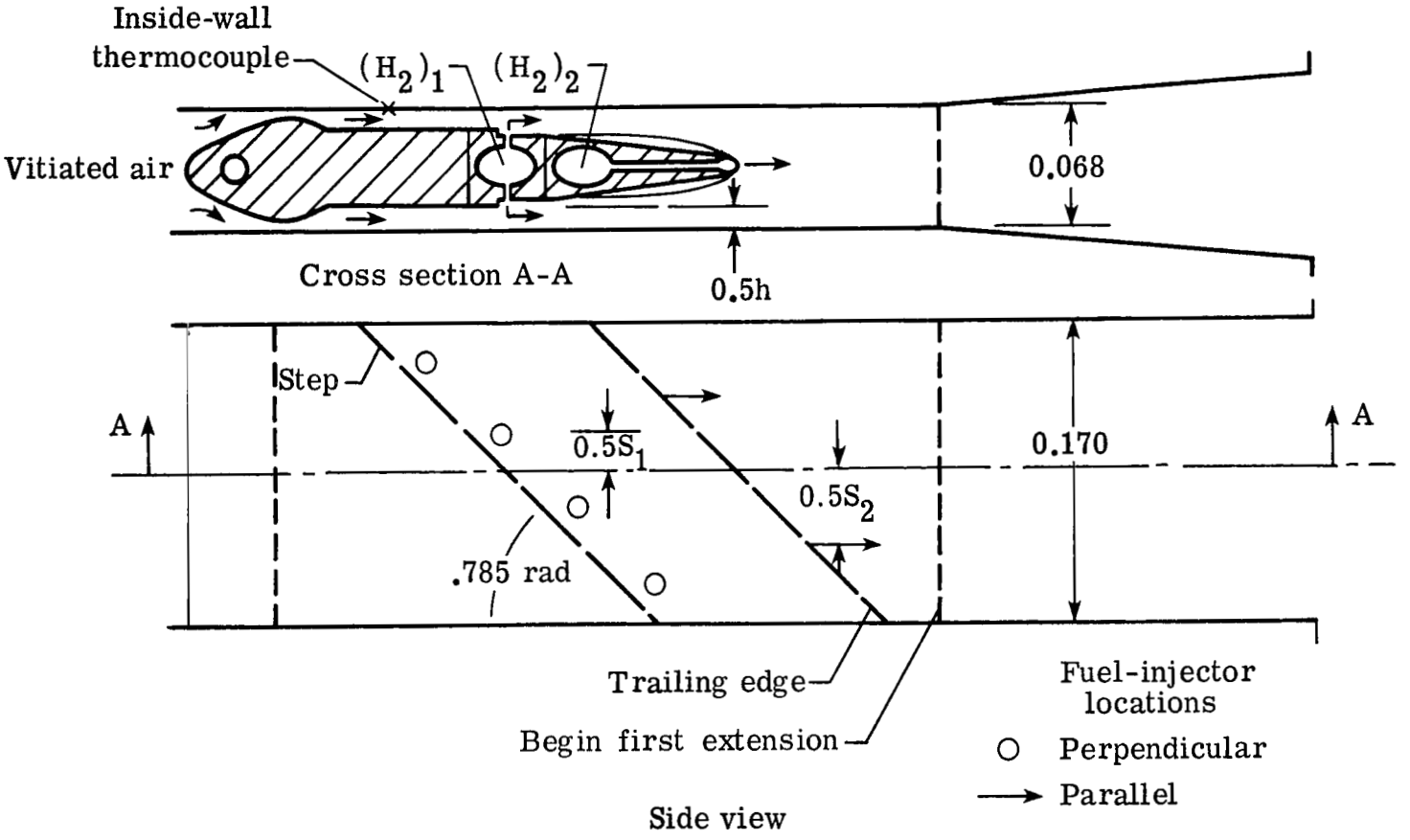

(a) Combustor-model details.

Figure 6.- Swept-strut combustor. All dimensions are in meters.

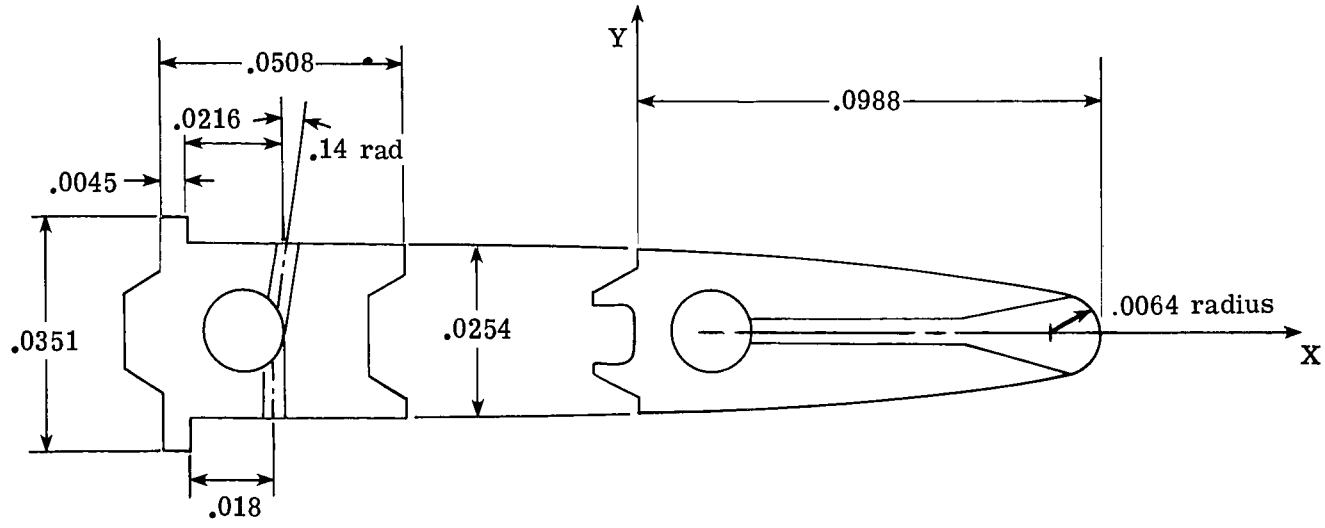

Perpendicular injectors
$d_1 = 0.0016$
$S_1 = 0.0424$
$x_s = 0.0216/0.0180$
$n_1 = 8$
$h_s = 0.0048$

Parallel injectors
$d_2 = 0.0049$
$S_2 = .0849$
$n_2 = 2$

X	± Y
0.000	0.0127
.0127	.0122
.0254	.0115
.0381	.0106
.0508	.0098
.0635	.0088
.0762	.0077
.0889	.0065

(b) Injector block details.

Figure 6.- Concluded.

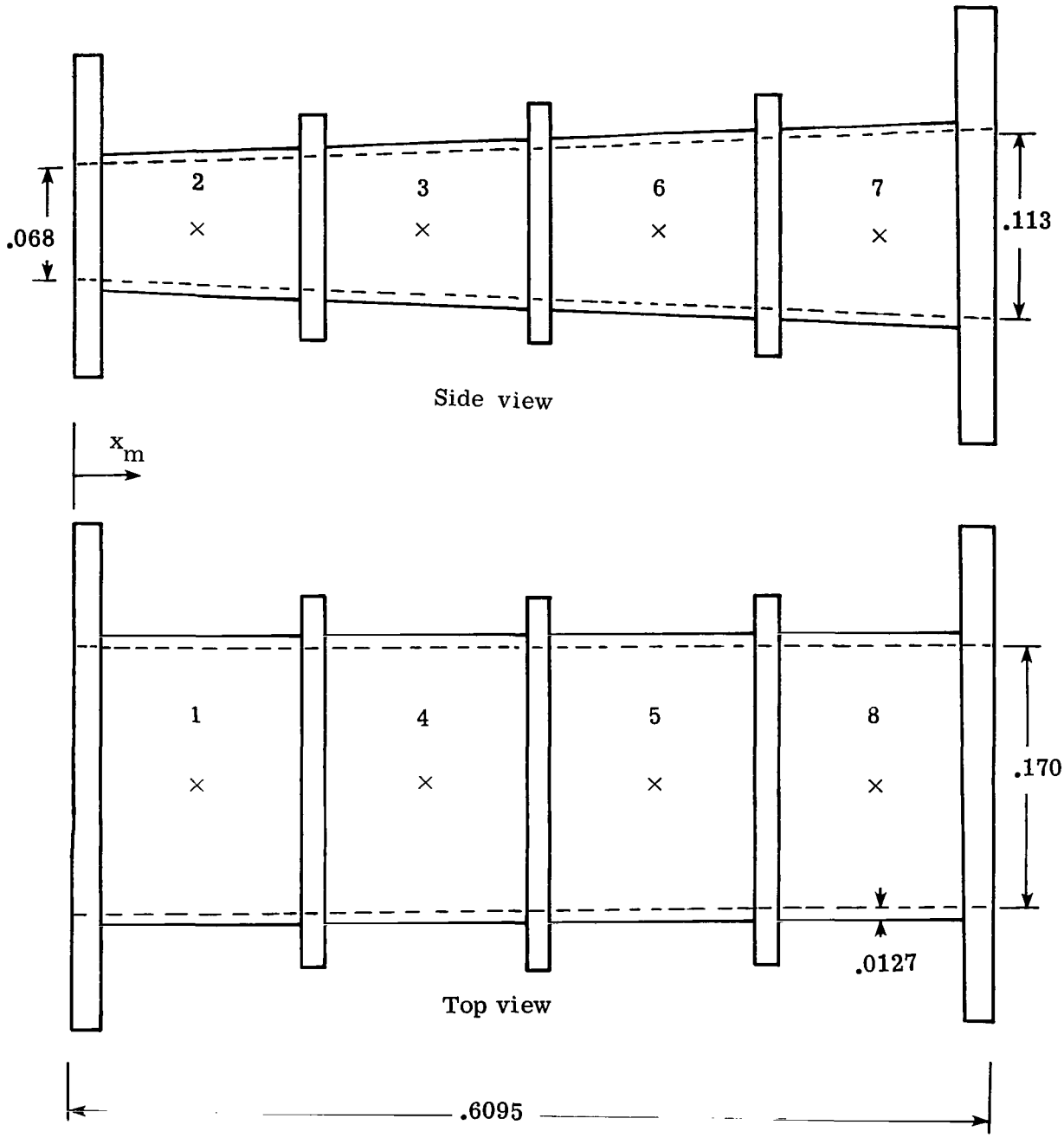

Figure 7.- Model extension. All dimensions are in meters.

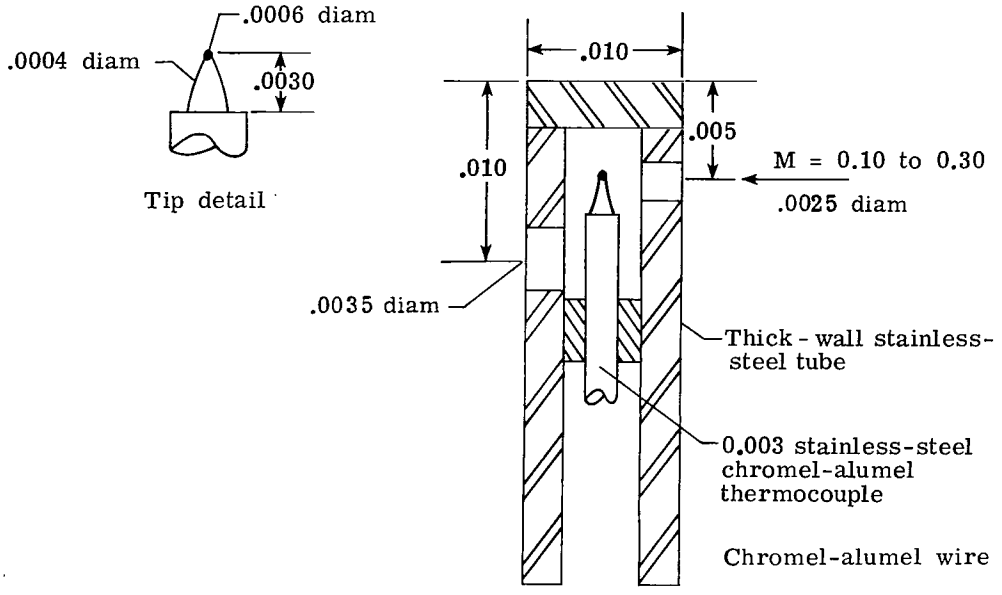

(a) Probe detail.

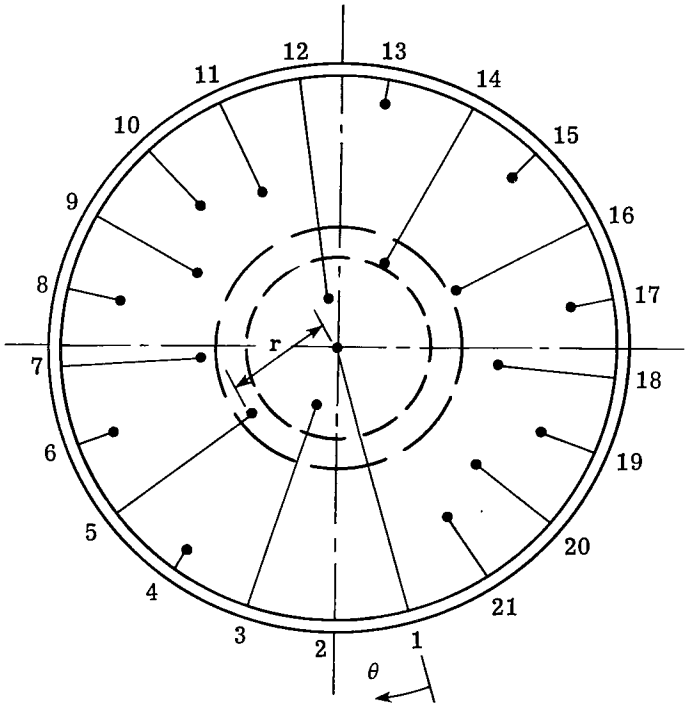

(b) Probe location.

Figure 8.- Calorimeter total-temperature probes. All dimensions are in meters.

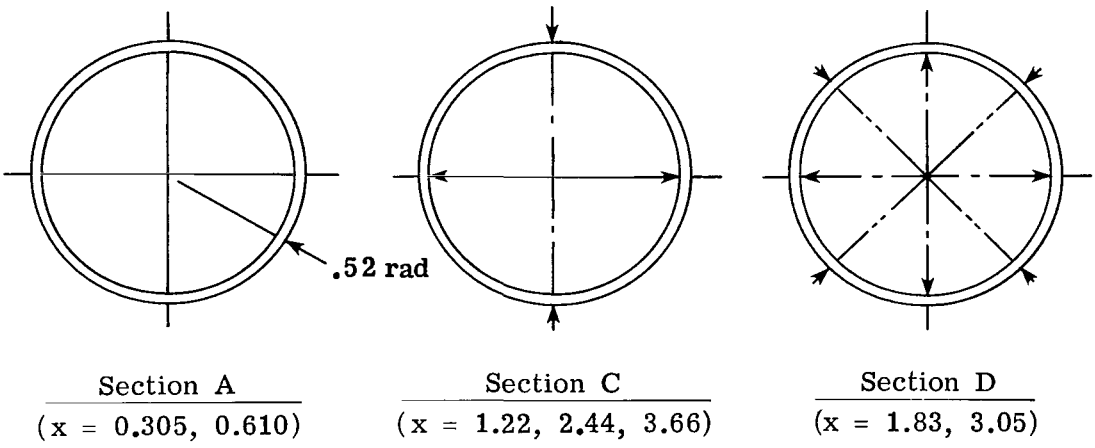

(a) Calorimeter thermocouple locations (view upstream).

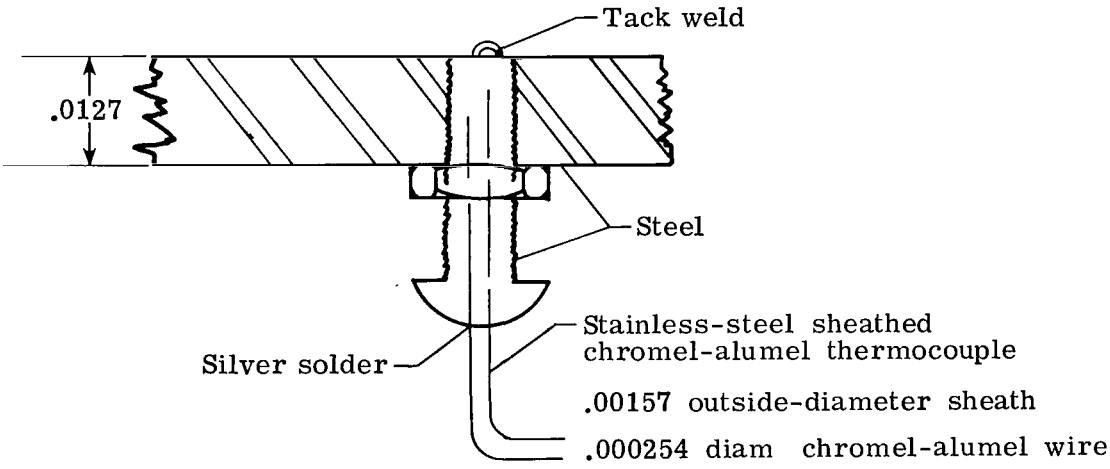

(b) Inside-wall thermocouple detail.

Figure 9.- Calorimeter-wall thermocouples. All dimensions are in meters.

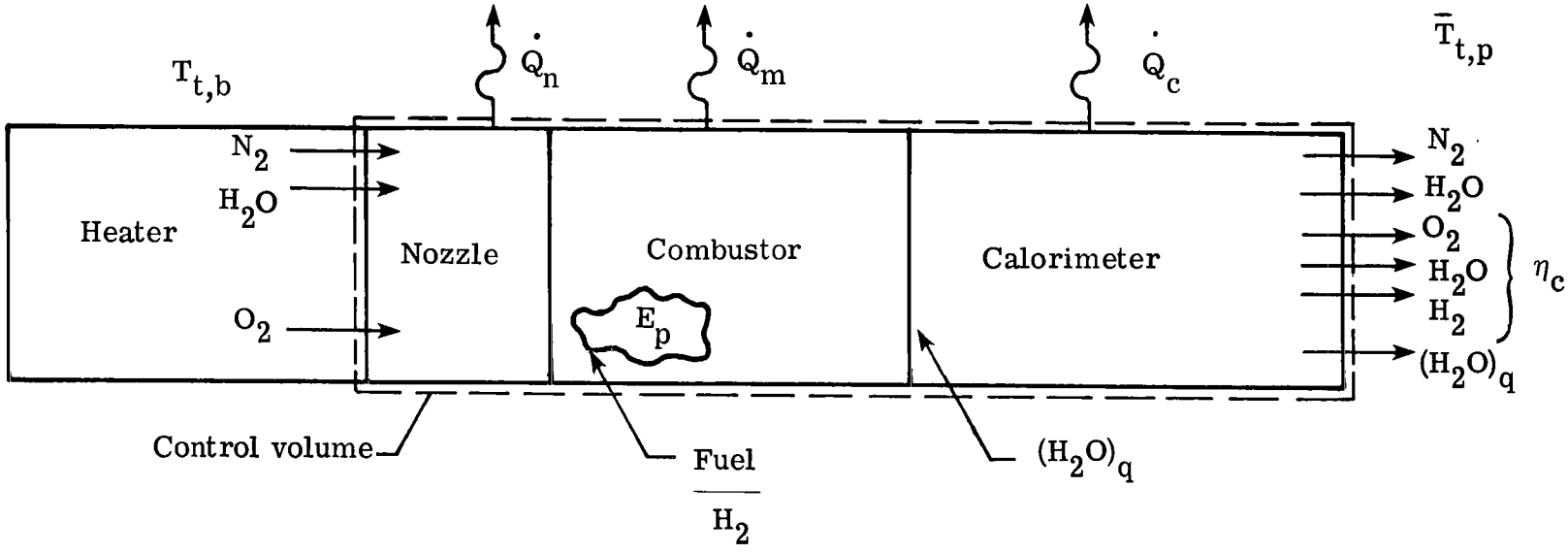

Figure 10.- Schematic of calorimetric balance.

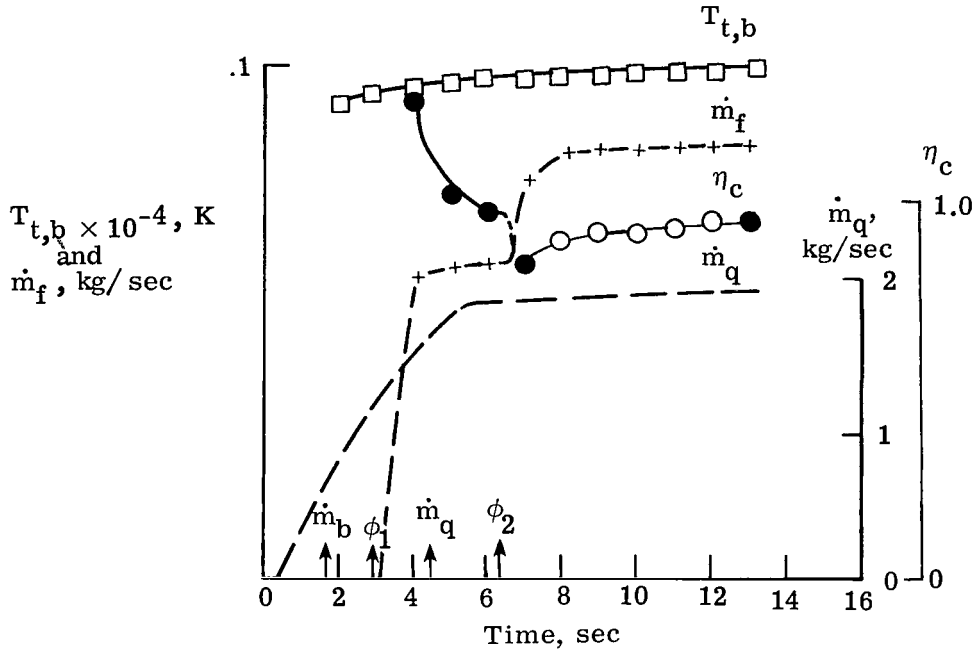

(a) Test conditions.

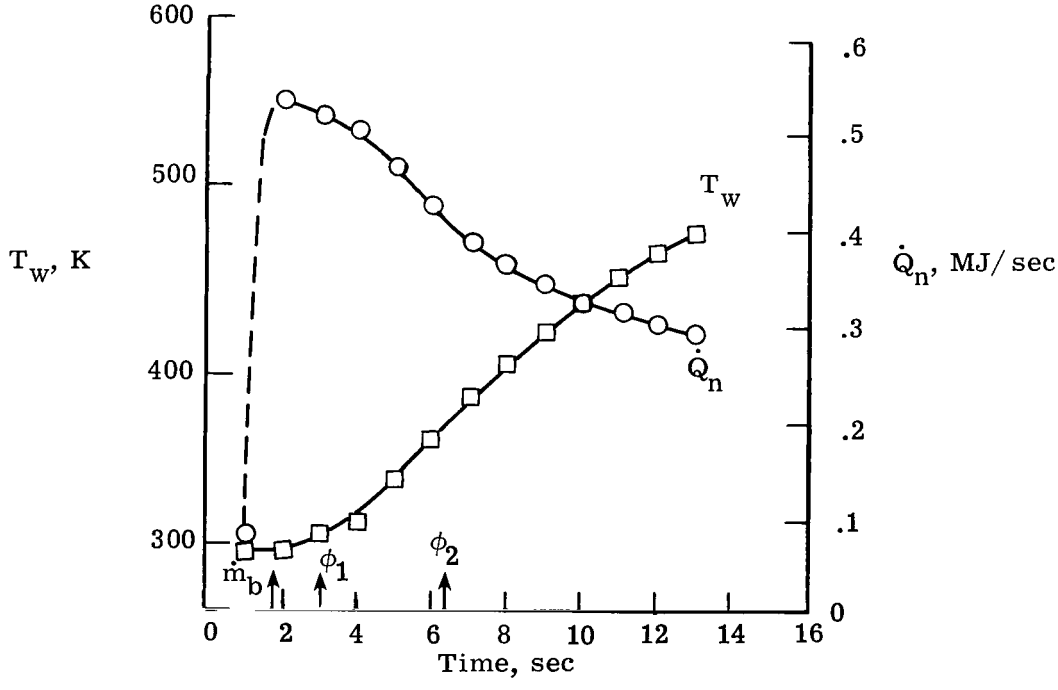

(b) Nozzle response: wall temperature and heat flux.

Figure 11.- Typical calorimeter results.

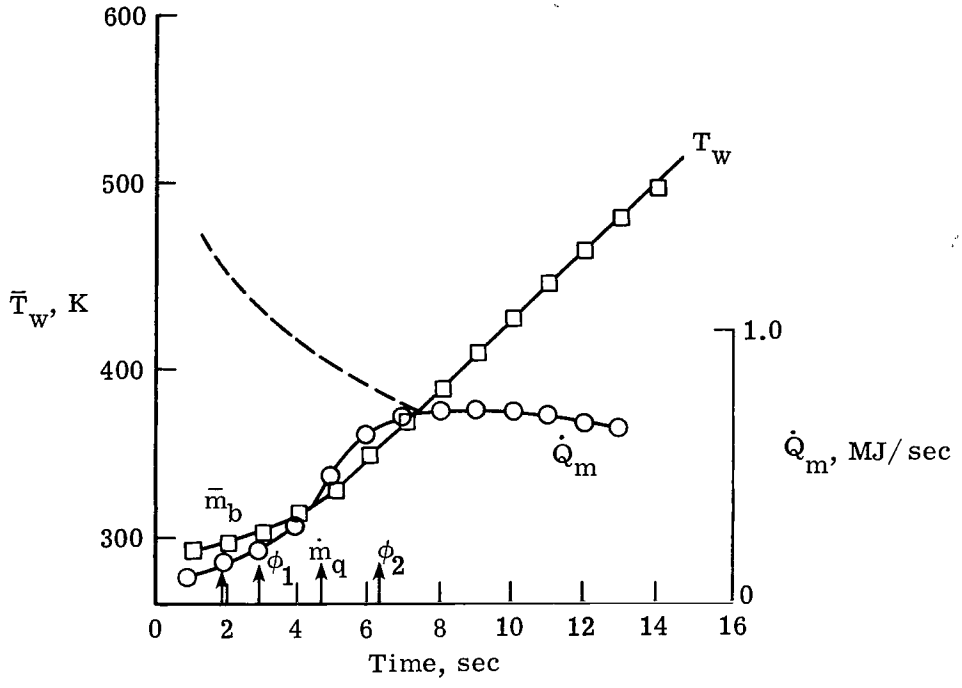

(c) Model response: wall temperature and heat flux.

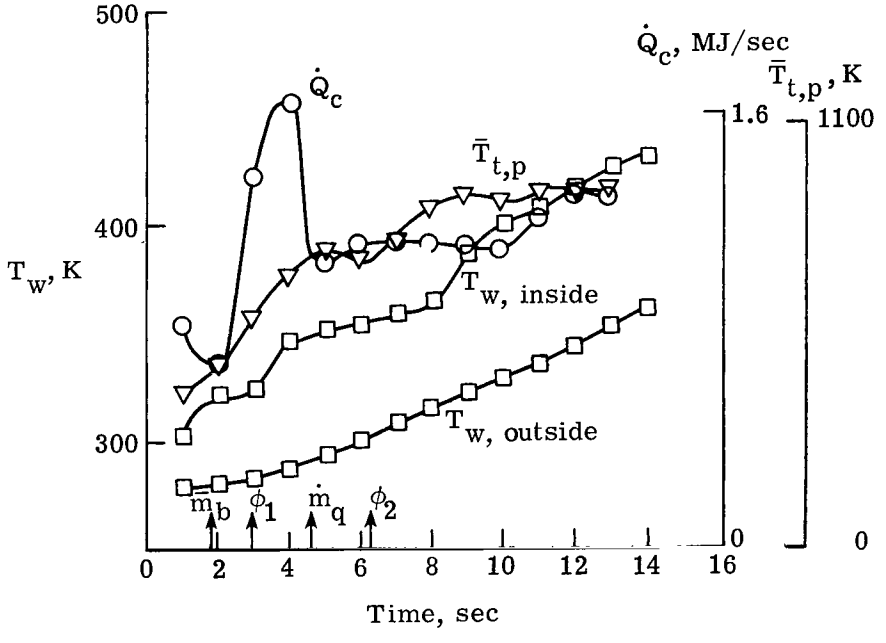

(d) Calorimeter response.

Figure 11.- Concluded.

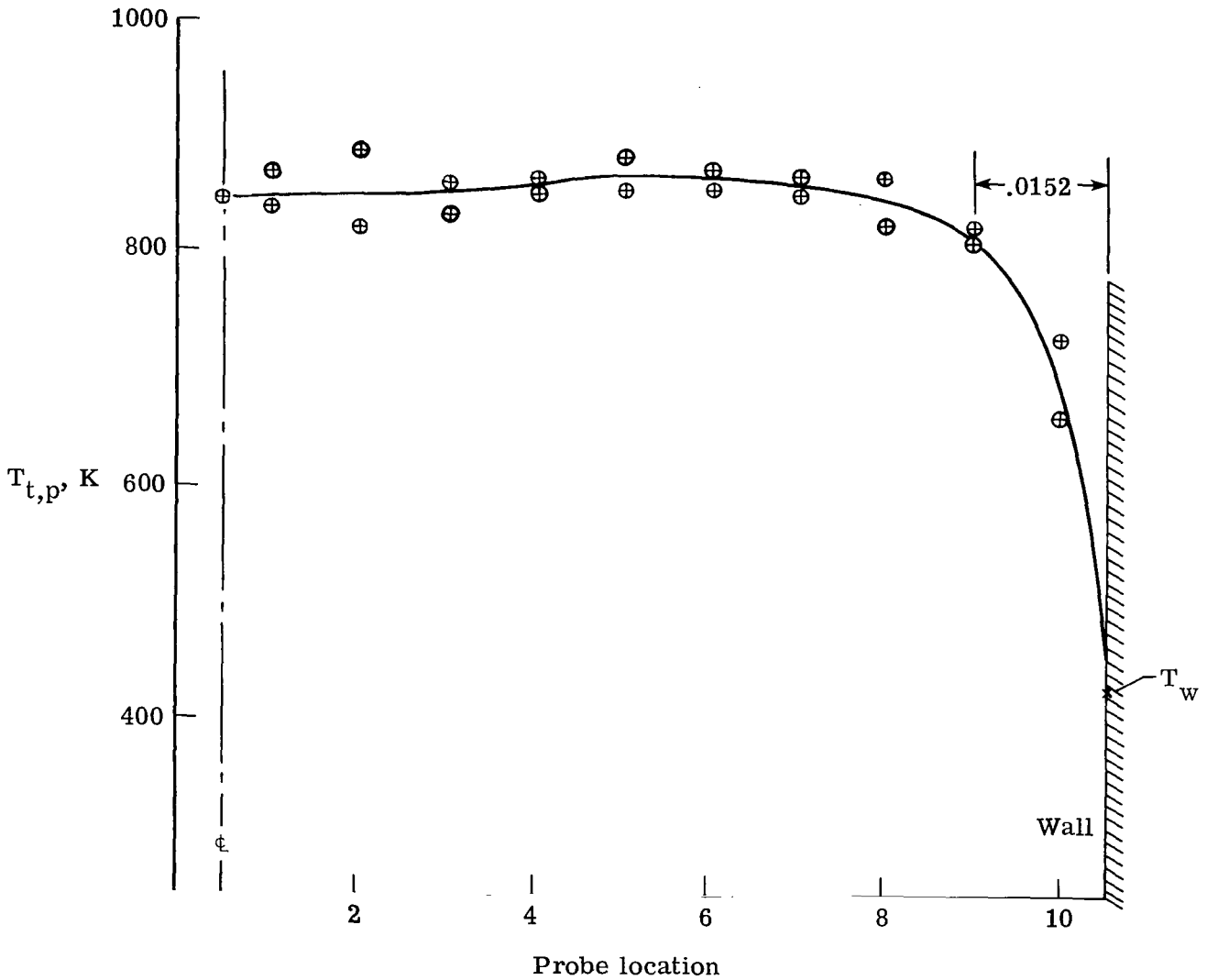

Figure 12.- Total-temperature profile at calorimeter exit.

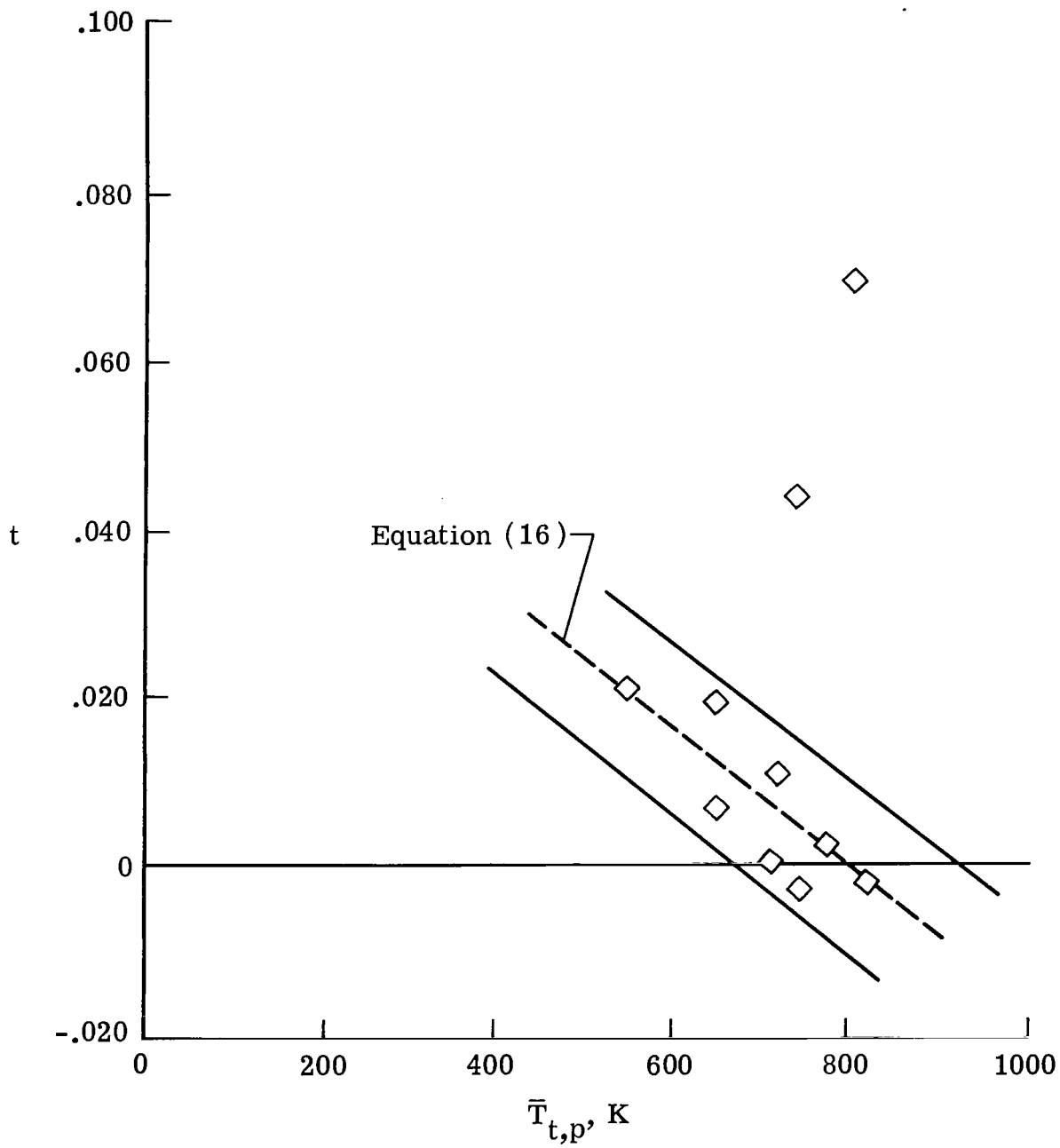

Figure 13.- Dependence of calorimeter tare on calorimeter total temperature.

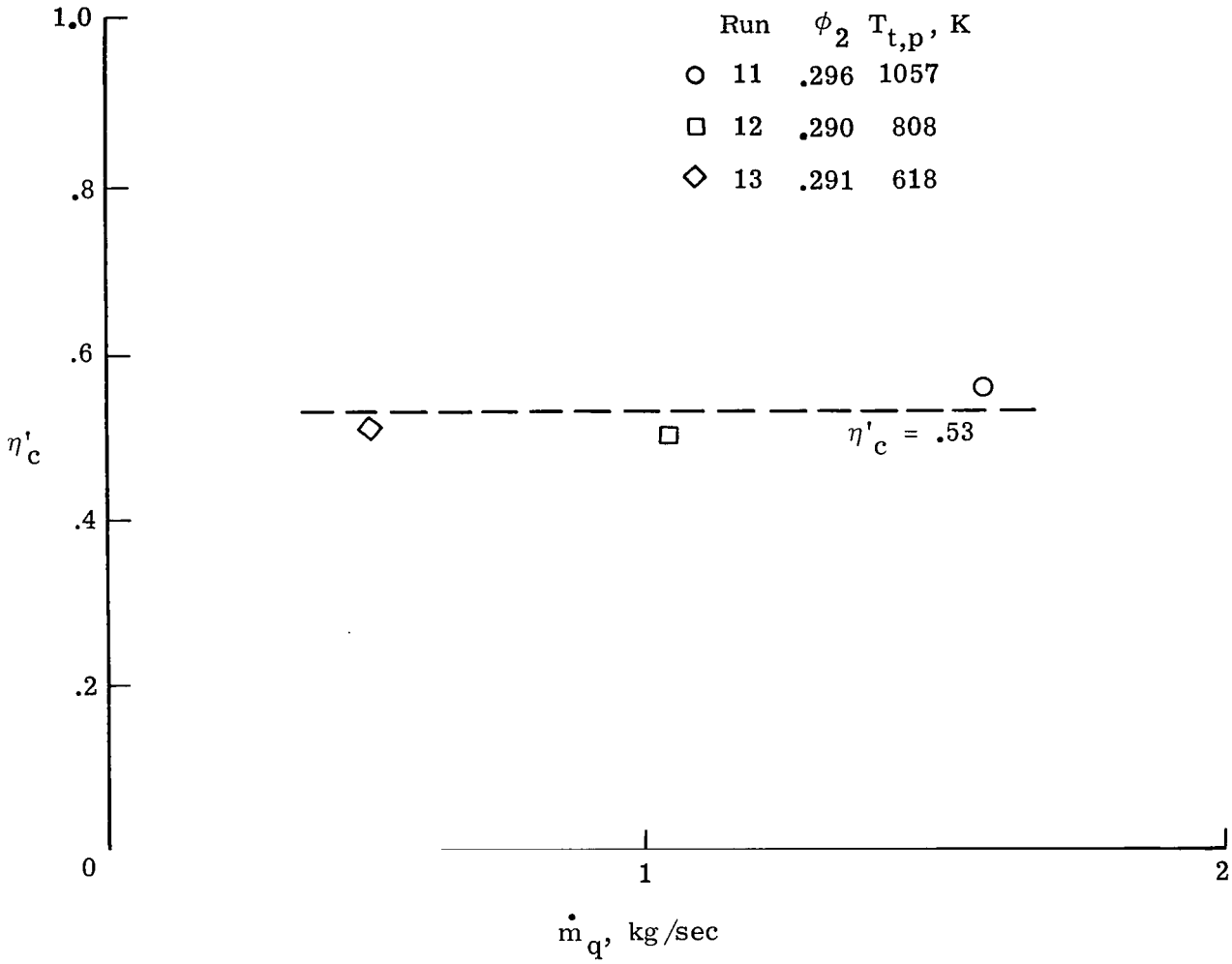

Figure 14.- Effect of quench-water flow on η'_c. $\phi_1 = 0$, $T_{t,b} \approx 1425$ K, $P_{t,b} \approx 0.66$ MPa.

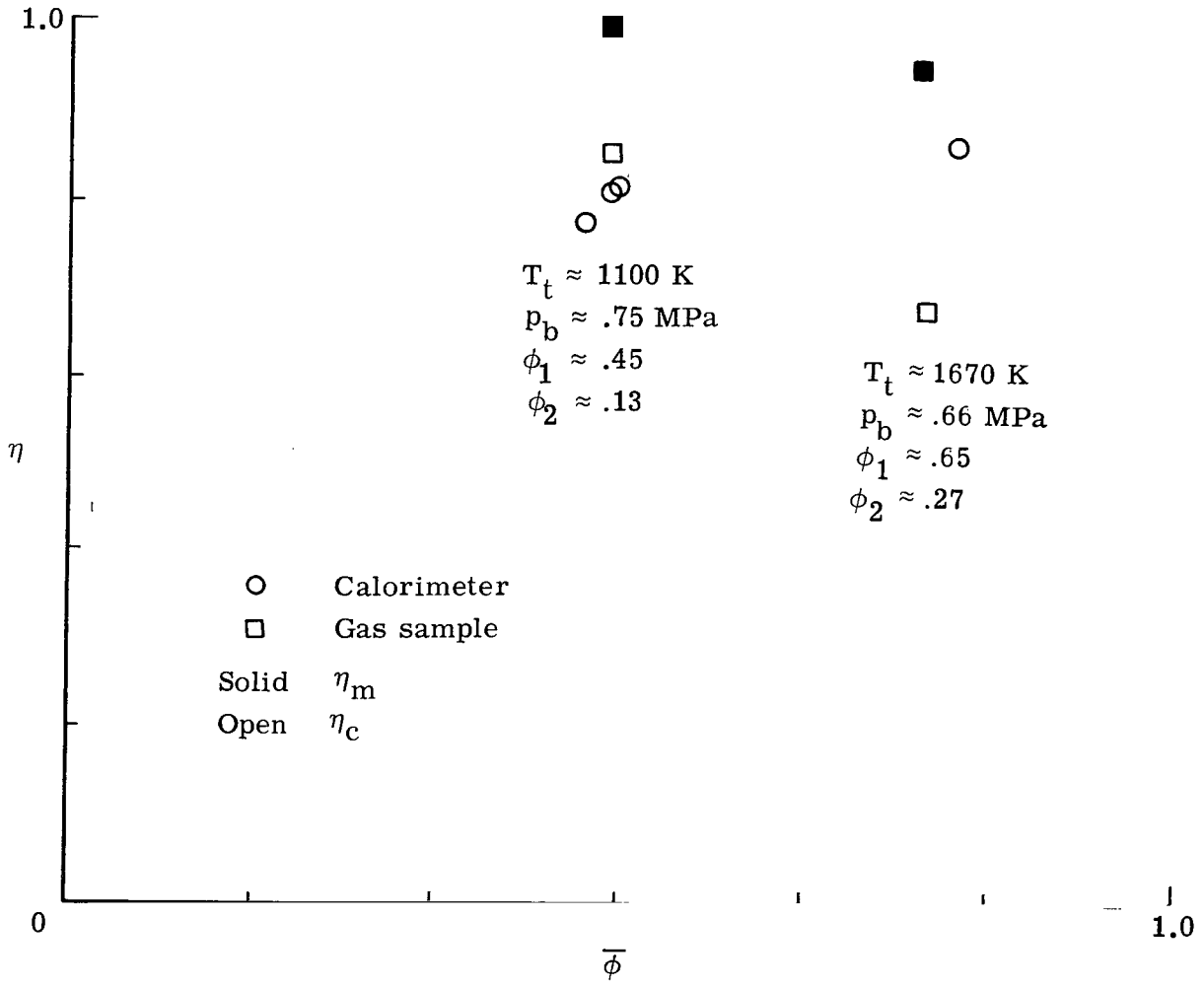

Figure 15.- Comparison of gas-sample and calorimeter results.

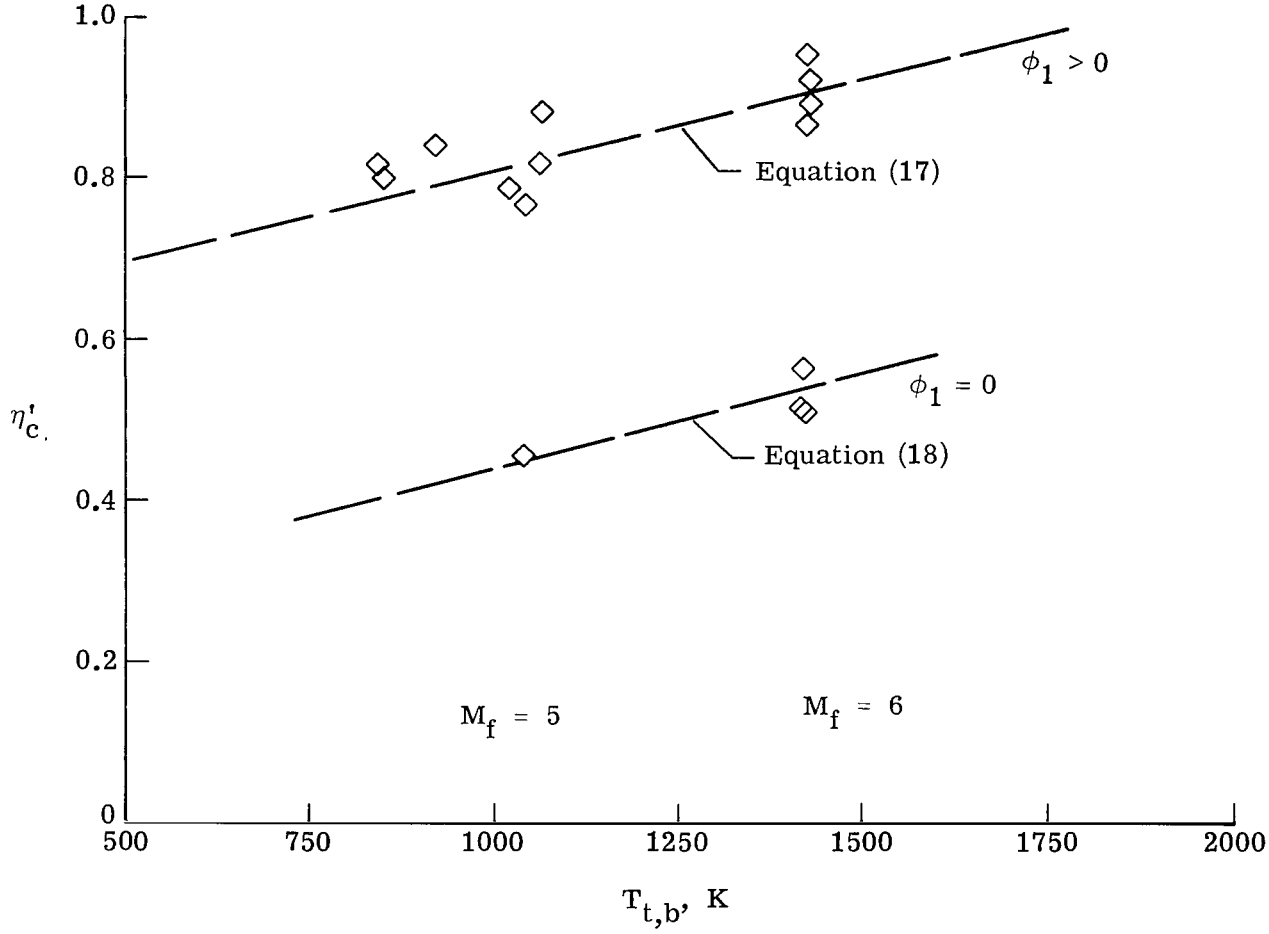

Figure 16.- Variation of η'_c with burner temperature.

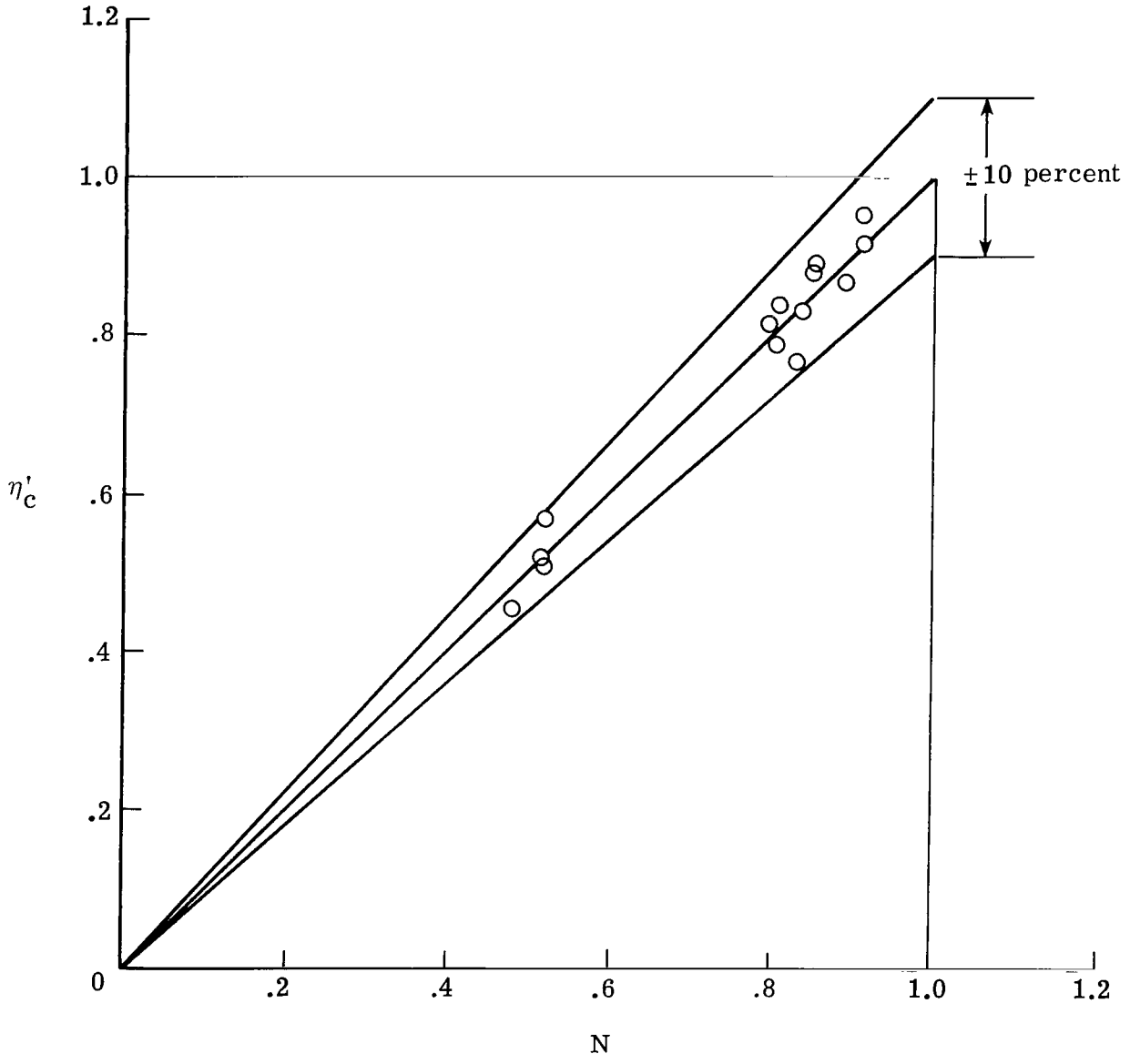

Figure 17.- Combustion efficiency for swept-strut model.

1. Report No.	2. Government Accession No.	3. Recipient's Catalog No.
NASA TP-1739		

4. Title and Subtitle	5. Report Date
EVALUATION OF A BULK CALORIMETER AND HEAT BALANCE FOR DETERMINATION OF SUPERSONIC COMBUSTOR EFFICIENCY	December 1980
	6. Performing Organization Code 505-32-93-01

7. Author(s)	8. Performing Organization Report No.
C. R. McClinton and G. Y. Anderson	L-13943
	10. Work Unit No.

9. Performing Organization Name and Address	11. Contract or Grant No.
NASA Langley Research Center Hampton, VA 23665	

12. Sponsoring Agency Name and Address	13. Type of Report and Period Covered
National Aeronautics and Space Administration Washington, DC 20546	Technical Paper
	14. Sponsoring Agency Code

15. Supplementary Notes

16. Abstract

Results are presented from the shakedown and evaluation test of a bulk calorimeter. The calorimeter is designed to quench the combustion at the exit of a direct-connect, hydrogen-fueled, scramjet combustor model, and to provide the measurements necessary to perform an analysis of combustion efficiency. Results indicate that the calorimeter quenches reaction, that reasonable response times are obtained, and that the calculated combustion efficiency is repeatable within ±3 percent and varies in a regular way with combustor model parameters such as injected fuel-equivalence ratio.

17. Key Words (Suggested by Author(s))	18. Distribution Statement
Calorimetry Scramjet Combustion diagnostics	Unclassified - Unlimited Subject Category 07

19. Security Classif. (of this report)	20. Security Classif. (of this page)	21. No. of Pages	22. Price
Unclassified	Unclassified	42	A03

For sale by the National Technical Information Service, Springfield, Virginia 22161

NASA-Langley, 1980

National Aeronautics and Space Administration

Washington, D.C.
20546

Official Business
Penalty for Private Use, $300

THIRD-CLASS BULK RATE

Postage and Fees Paid
National Aeronautics and Space Administration
NASA-451

U.S.MAIL

9 1 1U,A, 121280 S00903DS
DEPT OF THE AIR FORCE
AF WEAPONS LABORATORY
ATTN: TECHNICAL LIBRARY (SUL)
KIRTLAND AFB NM 87117

NASA

POSTMASTER: If Undeliverable (Section 158 Postal Manual) Do Not Return